Title

VARIATION OF NEUTRON TOTAL CROSS SECTION OF BISMUTH AND URANIUM BETWEEN 45 AND 160 MeV

Author

Linlor, William I.

Publication Date

1953-07-30

Thesis/dissertation

UNIVERSITY OF CALIFORNIA

Radiation Laboratory

BERKELEY, CALIFORNIA

DISCLAIMER

UCRL-2303
Unclassified-Physics Distribution

UNIVERSITY OF CALIFORNIA

Radiation Laboratory

Contract No. W-7405-eng-48

VARIATION OF NEUTRON TOTAL CROSS SECTION OF BISMUTH AND URANIUM BETWEEN 45 AND 160 MEV

William I. Linlor

(Thesis)

July 30, 1953

Berkeley, California

TABLE OF CONTENTS

LIST OF TABLES

LIST OF FIGURES

VARIATION OF NEUTRON TOTAL CROSS SECTION OF BISMUTH AND URANIUM BETWEEN 45 AND 160 MEV

William I. Linlor

(Thesis)

Radiation Laboratory, Department of Physics
University of California, Berkeley, California

July 30, 1953

ABSTRACT

The variation of neutron total cross section with energy of bismuth and uranium between 45 and 160 Mev has been measured with a time-of-flight instrumentation in a good geometry transmission experiment. Bismuth shows a dip in cross section to 4.14 ± 0.14 barns at 62 Mev, followed by a rise to 4.92 ± 0.12 barns at 70 Mev. Uranium shows a dip in cross section to 4.53 ± 0.17 barns at 62 Mev, followed by a rise to 5.30 ± 0.15 barns at 70 Mev.

The points for both bismuth and uranium show the same general variation with energy as the data first obtained by Taylor and Wood[6,7] for lead. Variation of neutron total cross section with energy for carbon also was measured with the same instrumentation as a check. The results agree well with values published by others.[7]

As part of the data, the direct beam neutron spectrum has been measured; it seems to agree with the theoretical curve given by Serber[3] for an "opaque-nucleus" model with 195 Mev deuterons being stripped on a "thin" target.

VARIATION OF NEUTRON TOTAL CROSS SECTION OF BISMUTH AND URANIUM BETWEEN 45 AND 160 MEV

William I. Linlor

(Thesis)

Radiation Laboratory, Department of Physics
University of California, Berkeley, California

July 30, 1953

INTRODUCTION

The purpose of this research is the experimental determination of the variation of the total attenuation cross section with energy for neutrons in materials of high atomic number, in the 100 Mev region. For reasons to be mentioned later in this section, the materials used were bismuth and uranium.

It would be desirable to discuss in detail the relation of this research to the general field of neutron physics. However, at the present time the state of theory in regard to nuclear forces seems to be undergoing modification. Keeping this in mind, we merely summarize the relations which approximately describe neutron behavior in the various energy regions.

Very slow neutrons can be diffracted by nuclei arranged in planes, in accordance with the well-known Bragg condition:

$$n\lambda = 2d \cos \theta$$

$$\lambda = h/Mv$$

(Meaning of symbols in given in Section XII, "Nomenclature.")

Values of λ for representative energies are given in Table 1, though of course only for values of λ of the order of 10^{-8} cm. does the diffraction occur.

Table 1

Neutron Energy and de Broglie Wave Length

Energy	$\lambda\!\!\!^{-}$ (approximate)
kT (20° C)	2.86×10^{-9} cm.
1 ev	4.55×10^{-10} cm.
1 Mev	4.55×10^{-13} cm.
100 Mev	4.55×10^{-14} cm.

In the region of an energy resonance, resonance theory is employed. An approximate expression for the cross section for a particular (α, β) reaction is given by the Breit-Wigner[1] one-level relation. In the notation of Blatt and Weisskopf[2] with the effect of spins and other refinements neglected:

$$\sigma_\ell (\alpha, \beta) \cong (2\ell + 1)\, \pi\, \lambda\!\!\!^{-2}_\alpha \frac{\Gamma^s_\alpha \Gamma^s_\beta}{(\epsilon_\alpha - \epsilon_{\alpha s})^2 + (\frac{1}{2}\Gamma^s)^2}$$

Elastic scattering is described by:

$$\sigma_\ell (\alpha, \alpha) = (2\ell + 1)\, \pi\, \lambda\!\!\!^{-2}_\alpha \left| \frac{i\,\Gamma^s_\alpha}{(\epsilon_\alpha - \epsilon_{\alpha s}) + \frac{1}{2} i\,\Gamma^s} + A^\ell_{pot} \right|^2$$

For a capture reaction, with emission of a gamma ray:

$$\sigma_{cap}\ (\alpha) = (2\ell + 1)\, \pi\, \lambda\!\!\!^{-2}_\alpha \frac{\Gamma^s_\alpha \Gamma^s_{rad}}{(\epsilon_\alpha - \epsilon_{\alpha s})^2 + (\frac{1}{2}\Gamma^s)^2}$$

For neutron energies not near a resonance and up to tens of Mev, the theory of the compound nucleus is employed. This is based on the assumption, due to Bohr, that the mode of disintegration of a compound nucleus depends only on its energy, angular momentum,

and parity. The manner in which it had been produced is irrelevant, because the incoming particle is presumed to be "mixed thoroughly" with the other particles in the nucleus before any decays occur. A further assumption of the compound nucleus theory is that the characteristic properties of nuclear matter are maintained even if the nucleus is excited so highly that it is capable of emitting particles. In terms of energy levels, one might say that the density of states of the compound nucleus is very high, so that the level widths overlap each other.

There are two other assumptions regarding the nucleus which are needed to obtain cross sections on the continuum theory:

a) The nucleus has a well-defined surface which is a sphere of radius R.

b) When the particle is inside the nuclear surface, it moves with an average kinetic energy which is much higher than its energy outside.

A mathematical outline of a method of calculation, again using the notation of Blatt and Weisskopf,[2] follows.

For large values of kr:

$$\exp(i k z) \cong \frac{\sqrt{\pi}}{kr} \sum_{\ell=0}^{\infty} \sqrt{2\ell+1}\; i^{\ell+1} \left\{\exp\left[-i\left(kr - \frac{1}{2}\ell\pi\right)\right] - \exp\left[+i\left(kr - \frac{1}{2}\ell\pi\right)\right]\right\} Y_{\ell,0}$$

$$k = \frac{1}{\lambda\!\!\!^{-}} = \frac{1}{\hbar}\sqrt{2ME}$$

$$\psi(\bar{r}) \cong \frac{\sqrt{\pi}}{kr} \sum_{\ell=0}^{\infty} \sqrt{2\ell+1}\; i^{\ell+1} \left\{\exp\left[-i\left(kr - \frac{1}{2}\ell\pi\right)\right] - \eta_{\ell} \exp\left[+i\left(kr - \frac{1}{2}\ell\pi\right)\right]\right\} Y_{\ell,0}$$

$$\psi_{scatt} = \psi(\bar{r}) - \exp(i k z)$$

$$= \frac{\sqrt{\pi}}{kr} \sum_{\ell=0}^{\infty} \sqrt{2\ell + 1}\ i^{\ell+1} (1 - \eta_\ell) \exp\left[+ i \left(kr - \frac{1}{2}\ell\pi\right)\right] Y_{\ell,0}$$

The scattering cross section is obtained by dividing the number of scattered particles per second by the number of incident particles per square centimeter per second. This leads to:

$$\sigma_{sc,\ell} = \pi \lambda\!\!\!^{-2} (2\ell + 1) \left|1 - \eta_\ell\right|^2$$

The reaction cross section is obtained by dividing the number of particles taken out of the beam per second by the number of incident particles per square centimeter per second, and yields:

$$\sigma_{r,\ell} = \pi \lambda\!\!\!^{-2} (2\ell + 1)(1 - \left|\eta_\ell\right|^2)$$

The determination of η_ℓ involves the solution of the Schroedinger equation, and becomes:

$$\eta_\ell = \frac{f_\ell - \Delta_\ell + i s_\ell}{f_\ell - \Delta_\ell - i s_\ell} \exp(2i \xi_\ell)$$

The result for the total cross section of a nucleus is the sum of σ_r and σ_{sc}:

$$\sigma_r = \pi \lambda\!\!\!^{-2} \sum_{\ell=0}^{\infty} (2\ell + 1) \frac{4 s_\ell R (k + k_1)}{\Delta_\ell^2 + [R (k + k_1) + s_\ell]^2}$$

$$\sigma_{sc} = \pi \lambda\!\!\!^{-2} \sum_{\ell=0}^{\infty} (2\ell + 1) \left| \frac{2i s_\ell}{\Delta_\ell + i [R (k + k_1) + s_\ell]} + \exp(- 2 i \xi_\ell) - 1 \right|^2$$

For values of $kR \gtrsim 4$, the total cross section is close to the value for a perfectly reflecting sphere.

At neutron energies in the range of 100 Mev, the mean free path of the incident neutron within the nucleus is of the same order of magnitude as the nuclear radius. An incident neutron may leave the bombarded nucleus after a few internal collisions with nucleons--certainly without the "thorough mixing" necessary for the idea of a compound nucleus to apply. (The mean free path is presumed to be the same in all nuclei because of the constant density of nuclear matter.) This "transparency" effect[3] has led to the development of an optical model of the nucleus by Fernbach, Serber, and Taylor.[4] They regard the nucleus as a sphere of nuclear matter of uniform density, having an absorption coefficient K, radius R, and an index of refraction determined by the mean potential energy, V, of the neutron in the nucleus.

$$k = \frac{1}{\hbar}\sqrt{2\,M\,E} = 1/\lambda\!\!\!^{-}$$

$$k + k_1 = k\,(1 + V/E)^{1/2}$$

$$K = \frac{3}{4\,\pi\,R^3}\,A\,\sigma$$

$$\sigma = \frac{1}{A}\left[Z\,\sigma_{np} + (A - Z)\,\sigma_{nn}\right.$$

For $E = 90$ Mev, $k = 2.08 \times 10^{13}$ cm^{-1}.

For $R = 1.37\,A^{1/3} \times 10^{-13}$ cm, the Fermi energy is 22 Mev, and V is about 30 Mev. This gives $k_1 = 3.22 \times 10^{12}$ cm^{-1}.

A wave going a distance T in nuclear matter has an amplitude and relative phase

$$a = a_o \exp\left(-\frac{1}{2} K + i k_1\right) T$$

Using the above relations, Fernbach, Serber, and Taylor[4] calculate for a spherical nucleus

$$\sigma_a = \pi R^2 \{1 - [1 - (1 + 2 K R) \exp(-2 K R)]/2 K^2 R^2\}$$

$$\sigma_a = 2\pi \int_o^R \left|1 - \exp(-K + 2i k_1) s\right|^2 \rho \, d\rho$$

$$\sigma_t = \sigma_a + \sigma_d$$

From these expressions they obtain calculated values of R which, when plotted against $A^{1/3}$ yield essentially a straight line, using experimentally-determined values of total cross section. Values of k_1 and K are chosen so as to give the best straight line fit. The result for R is

$$R = 1.37 A^{1/3} \times 10^{-13} \text{ cm.}$$

Up to this point the various theoretical treatments seem reasonably satisfactory for the associated energy ranges. With the development of more refined experimental methods both in low and high energy regions, however, results have been obtained which do not seem to admit of explanation on the basis of theories described.

Considering experimental cross sections for neutrons having energies in the vicinity of 270 Mev, one has to set $k_1 = 0$ to get an approximate fit of experimental data with the transparent model; this implies that at such an energy a neutron experiences no potential change on entering the nucleus. For neutron energies between about 50 Mev and 270 Mev, the results of DeJuren and Moyer[5] show that the total cross section for carbon, aluminum, copper, and lead plotted against neutron energy drops rather abruptly in the region of 100 Mev, and flattens to a slowly-varying region at about 200 Mev.

More unexpected rsults were recently obtained by Taylor and Wood[6,7] in measurement of the total neutron cross section for lead with apparatus having relatively sharp energy resolution. They find a "dip" in the total neutron cross section at about 60 Mev, followed by a maximum at about 80 Mev. Similar dips, though not as pronounced, seem to be present in their results for copper and cadmium at about 30 to 40 Mev.

Calculations are in progress by members of the theoretical section of UCRL using electronic computers to see if the optical model can reproduce the high-energy experimental results, using whatever parameters are necessary.

A version of the optical-model approach to the problem has been employed recently also by V. F. Weisskopf.[8] The "old" picture of strong interaction of an incoming nucleon with the other particles of the nucleus is equivalent, in optical language, to assuming that the nucleus is black--the incoming nucleon has zero mean free path. Weisskopf proposes, still speaking in optical language, that the nucleus be considered to be a cloudy crystal ball. The incoming nucleon is presumed to have a mean free path ℓ which is of the order of the nuclear radius R; the absorption coefficient is defined to be $K = \chi/\ell$. His initial theoretical results with this model seem promising.

One sees from these introductory comments, however, that the theoretical bases are being modified and developed to bring them into agreement with the new cross section evidence.

From the experimental point of view, it appeared desirable to confirm the results of Taylor and Wood, using an independent method if possible, and to obtain additional results for new elements. Because it seems that the "dip" is more pronounced in materials of high atomic number, this region is obviously the first place to search.

Boris Ragent and the writer, having developed a time-of-flight neutron spectrometer,[9] accordingly undertook the measurement of the variation of the total neutron cross sections with energy

in the 100 Mev region, paying particular attention to the energy resolution necessary for examination of variations in cross section for materials of high Z.

The results of the time-of-flight measurement for lead[10] confirm Taylor and Wood's dip.

To obtain information about possible dips in materials other than those investigated by Taylor and Wood, the present research is concerned with bismuth and uranium as scatterers. Concurrent research by Boris Ragent, using the same equipment, includes antimony and tantalum as scatterers.

Because the time-of-flight technique employed in this investigation has not been described in publication except in abstract form, the instrumentation will be described in considerable detail, particularly with respect to the checks which were made to insure that the instrumentation was working properly.

II PRINCIPLES OF THE EXPERIMENTAL METHOD

The basic requirement of a time-of-flight spectrometer is a burst of neutrons that occurs in an interval short compared to the time of flight. It is equally important that the detection interval be short compared to the time of flight; this latter requirement is relatively easy to meet with scintillation counters.

In Table 2 are given times of flight for neutrons of various energies, together with other related quantities. Times of flight are plotted versus energy in Fig. 1.

As finally developed, the system had a time resolution (full width at half maximum) of 0.7 shake, and a flight distance of 43.7 meters, yielding a resolving time (base of equivalent triangle denoting time uncertainty) of 3×10^{-10} second/meter. This is equivalent to a probable error in energy of ± 1.2 Mev at 90 Mev and 43.7 meters. A general description of the time-of-flight method follows.

The source is the "stripped-deuteron" beam of the 184-inch synchrocyclotron.[11, 12] By appropriate manipulation of the controls, one causes a single pulse of deuterons to be deflected onto an insulated probe placed inside the cyclotron. This probe is thick enough to stop the deuterons by ionization loss. Collection of charge on the probe, which produces a usable voltage pulse, and production of stripped neutrons occur simultaneously, resulting in a pulse of neutrons starting at a known place within a known time. In the path of the beam is placed a scintillator whose detection efficiency for neutrons is adjusted to give a desired counting rate.

A given pulse from the probe and the corresponding pulse from the scintillator, due to the detection of a neutron, are displayed, after fast amplification, on the sweep of an oscilloscope. If, for illustration, one takes all delays in the probe and signal lines to be equal, the separation in time of the two pulses on the oscilloscope sweep would represent the time of flight of a particular neutron.

Table 2

Neutron Energy and Time of Flight, etc.

Neutron Energy in Mev	β	Shakes* per meter	Shakes* for 43.7 meters	Energy uncertainty for 1 shake uncertainty at 43.7 meters	Probable Error** in Energy (for 0.2 shake uncertainty at 43.7 meters)
20	0.2032	1.6410	71.7	0.58	0.12
30	0.2468	1.3504	59.0	1.07	0.51
40	0.2829	1.1784	51.4	1.62	0.32
50	0.3139	1.0620	46.4	2.33	0.47
60	0.3413	0.9767	42.7	3.09	0.62
70	0.3659	0.9110	39.7	3.92	0.78
80	0.3883	0.8584	37.4	4.83	0.97
90	0.4089	0.8151	35.6	5.81	1.16
100	0.4279	0.7788	34.0	6.85	1.37
110	0.4457	0.7479	32.6	7.97	1.60
120	0.4623	0.7210	31.4	9.13	1.85
130	0.4778	0.6974	30.4	10.37	2.07
140	0.4925	0.6766	29.5	11.70	2.54
150	0.5064	0.6583	28.7	13.08	2.62
160	0.5195	0.6414	28.0	14.48	2.90
170	0.5319	0.6270	27.4	16.0	3.2
180	0.5438	0.6131	26.8	17.5	3.5
190	0.5551	0.6006	26.2	19.2	3.8
200	0.5659	0.5893	25.7	20.8	4.2
Gammas	1.000	0.3333	14.57		

* One shake = 10^{-8} second

** See section III F for basis on which probable error is obtained

A camera provides a photographic record of the sweeps. By use of a coincidence circuit actuated by the detected neutron, the oscilloscope trigger circuit is actuated only when an event has occurred, allowing the use of film speeds about 1/20 as fast as would be necessary if every probe pulse were photographed. The use of the oscilloscope and camera makes it possible to have all energy channels "open" at the same time. Subsequent film analysis determines the specific number of energy channels into which data are to be collected. The sweep is calibrated in time units by photographing a 50 MC sine wave. Energy calibration is accomplished by detection of gamma rays from the probe.

Let us now consider how cross sections are obtained with this system. Because the purpose of this research is the determination of the variation of total cross section with energy, no beam monitor is necessary. To see why this is so, let us note that when the deuterons are deflected to the probe, each pulse (or burst) contains a complete spectrum of neutrons. The spectrum is constant, providing there is no change in cyclotron operating conditions. After sampling the neutrons from a large number of probe bursts, the detector will have reproduced the energy spectrum (I_o) of the neutrons in the bursts, modified by the variation of detector efficiency with energy. Let us call this the I_oF spectrum, where F represents the factor involving varying detector efficiency with energy.

Interposing a scatterer in the beam in good geometry changes the spectrum as seen by the detector. Let us call this the I_1F spectrum. In obtaining the I_1F spectrum, let us for the moment assume that the I_o intensity (direct beam spectrum ahead of the scatterer) is constant, and that the running time is the same as for the I_oF case.

The cross section is therefore:

$$I_1F = I_oF \exp(-n\sigma_1)$$

$$\sigma_1 = \left(\frac{1}{n}\right) \ell n\, I_o/I_1 \qquad (1)$$

Now let us consider the effect of variation in deuteron beam current. An n-fold change in the number of deuterons striking the probe per second, which produce neutrons by stripping, results in an n-fold change in the rate of detecting neutrons at all energies. The shape of the $I_o F$ or $I_1 F$ spectrum is not affected by beam current variations. Suppose that the result of the variations is a spectrum that is A times as intense as the spectrum which would have been obtained if the beam current had been kept constant. Then Eq. 1 becomes:

$$\sigma_1 = (1/n)\ \ell n\ A\ I_o/I_1 = (1/n)(\ell n\ A + \ell n\ I_o/I)$$

Obviously the ln A term does not affect the variation of σ_1 with energy.

Inasmuch as the dip, if any, in the cross section for bismuth and uranium is of main interest, a modification can be made in the usual procedure for obtaining cross section data, resulting in considerable saving in cyclotron running time. The modification is the direct comparison of lead (for which the cross section is now presumed known) with the two unknown materials, without recourse to unattenuated beam (I_o) data. To illustrate the point, suppose that we have two mean free paths of each of the three elements, and have obtained the respective spectra (discarding the factor F that denotes variation of detector efficiency with energy) designated by I_{Pb}, I_{Bi}, and I_U. If all three spectra have the same shape, the elements have the same variation of cross section with energy. (We presume that the I_o spectrum is the same for all three, which is assured by interchanging the scatterers during the run without distrubing the cyclotron conditions in any way.)

The saving in running time arises as follows: As will be discussed in a later section (Section III G), the maximum rate of taking data, without jamming, is about 3 counts per second. If

one had to take an I_o spectrum at this maximum rate, then the I_{Bi} and I_U spectra would come in at a rate $1/e^2$ as fast. But by using lead as the comparison material, one can adjust the counting rate so that all three spectra come in at the maximum rate, because no I_o rate is needed.

It is an important check on the accuracy of the experiment to obtain data on another element for which the cross section variation with energy is well known, and for which it is quite certain that no dip exists. Carbon was selected for this purpose.

III DETAILS OF EXPERIMENTAL METHOD

A. Geometrical Layout

The geometrical layout is shown in Fig. 2. All distances are measured from the probe along the beam axis, defined as the line between probe and scintillation detector. The forward cone of neutrons passes through the cyclotron tank wall, about one inch thick steel. It is collimated into a square beam with dimensions 7.6 cm x 7.6 cm by about two meters of concrete in the "igloo," whose center is 8 meters away from the probe. The hole in the main concrete shielding wall is sufficiently large so that no further collimation of the main beam takes place here.

The scatterer position is about 18 meters from the probe. A hole in the wall of the cyclotron building allows the beam to emerge. The scintillation detector is 43.7 meters away from the probe, the maximum convenient distance... it happens to be under the eaves of Radiation Laboratory Building 15, tucked away like the nest of an unjudicious bird. The scintillator consisted of a stilbene crystal with irregular dimensions, but approximately 1 cm x 0.5 cm area and 1.5 cm in the direction of the beam. Two 1P21 phototubes looked at it; the tubes were arranged so their axes were horizontal, and parallel to each other and to the beam.

Determination of the beam axis had to proceed by indirect means. A line was first established with a telescope by sighting on the counter and on the probe, the latter through a glass port in the cyclotron tank wall. This was a line tangent to the 81.0-inch radius of the cyclotron. The position of the probe during the runs was 83.8 inches, at which position it could no longer be seen through the glass port. Knowing the distance of the telescope from the probe, one could calculate the amount to move the telescope to place it on the beam axis. Using the telescope in this new position, one could now establish reference markers. Confirmation that the line of sight was indeed the axis was obtained during the run by placing a seven-foot long steel shaft, six inches in diameter, in position with its axis

coincident with the beam axis. Measurement of the scintillator counting rate versus shaft displacement parallel to the beam showed that the beam axis had been located to within ± 1/4 inch. Inasmuch as the scatterers were 6 inches x 6 inches area, this was sufficiently precise.

The four scatterers were interchanged manually every four minutes during the data runs, being mounted on a platform with wheels. The platform was pushed along a pair of rails; this could be done without having to turn off the beam. The direction of motion of the platform was 90° to the beam to within $\pm 0.3^{\circ}$, as measured by a telescope which could measure angles to 1 minute of arc. The place of the scatterers was perpendicular to the beam axis to within one degree, and perhaps closer. Since the cosine of 89° is 0.99985, this was sufficiently accurate.

B. Instrumentation and Electronics

A block diagram of the electronics is given in Fig. 3. A charge pulse due to the single burst of deflected deuterons occurs at the probe at the end of each modulation cycle (rate about 60 per second). This pulse, unamplified, is fed into a doubly-shielded cable (designation #21406) 150 feet long, leading to the counting area. Here the pulse is amplified by two Hewlett-Packard 460B amplifiers and by the amplifier which is built into the Tektronix #517 oscilloscope, ending on the positive y-axis deflecting plate. A suitable amount of delay is introduced into the "probe line." A detailed diagram of the electronics components is given in Fig. 4.

When a neutron produces a signal in the stilbene scintillator, the two 1P21 phototubes actuate a double-coincidence circuit, whose output, through a linear amplifier and blocking oscillator, triggers the oscilloscope. The voltage pulse from one of the 1P21 tubes is amplified, suitably delayed, and placed directly on the negative y-axis deflecting plate. Thus each sweep has a "probe pulse" and a "signal pulse" on it, the deflections being in opposite directions to avoid any possible confusion. A small number of sweeps occurs

because of neutrons having less than about 30 Mev energy, for which no probe pulse would be visible on the sweep. The coincidence circuit also ensures that only pulses having a height greater than a certain minimum will be counted, which facilitates film reading.

The sweep speed of 2×10^7 cm. per second is selected so that the entire desired neutron energy range in displayed on each sweep, as well as gamma ray photons when they occur. Because the scope is triggered by neutron-produced signals, all signal pulses come at essentially the same place near the start of the sweep. The probe pulses come at varying sweep distances: the less the time of flight, the greater is the separation of probe and signal pulses. For a gamma ray photon, the probe pulse comes nearly at the end of the sweep.

A General Radio camera using Linagraph Pan LP-420 35-mm film photographs the scope screen. The film runs steadily, with no shutter, at a speed determined by the average rate at which sweeps occur.

Time calibration is accomplished by placing a 50 MC sine wave on the scope, and photographing it under the same conditions as prevail during the experiment. Non-linearities due to sweep speed, film development, film projection, etc. are all compensated by the sine wave calibration.

For reference, it might be mentioned that the film is developed on a "Nikor" 100-foot reel without agitation in Atkinson A-72 developer, diluted with an equal amount of water, for 3 1/2 minutes at 20° C. The film is briefly swished through water, then fixed for 5 minutes in Kodak Acid Fixer, mixed in accordance with manufacturer's instructions.

The voltage on the 1P21 phototubes was kept constant at 1100 volts for at least 40 hours before the run, and was not turned off during the two-day run. It was obtained from a regulated power supply which is constant to about 0.5 percent. The scintillator was in a light-tight shield, and was not altered in position during the run.

The delays and amplification in the probe and signal lines were adjusted at the start of the run. Once the data runs were started no changes of any sort were made. Interchanging scatterers was done with beam on. Even distinguished visitors who wanted to see the cyclotron, and were escorted by a prominent member of the professorial staff, had the situation explained to them. The only interruption of data-taking was the unavoidable shut-down overnight.

C. Source of Neutrons

The source of neutrons is the stripped-deuteron beam[12] of the 184-inch synchrocyclotron. An insulated and shielded probe of copper is inserted into the cyclotron tank, tangent to the radius at a distance of 83.8 inches. This tangent line is also the beam axis, so that only neutrons in the forward direction are counted--the scintillator subtends a solid angle of about 3×10^{-8} steradians. The probe is long enough in the direction of the beam, 3.18 cm, to stop 195 Mev deuterons by ionization loss. The other dimensions are one inch in height and 1/16 inch radially. The shield around the probe consists of two flat pieces of copper sheet 0.010 inch thick. With glass and asbestos tape as insulating material, the built-up radial thickness of the probe is 1/4 inch. A schematic diagram of the probe is given in Fig. 5. Photographs of the shielded probe assembly which was used are shown in Fig. 6. Electrical connection from the probe to the external circuit is made through a Kovar seal. Doubly-shielded coaxial cable (#21406) carries the unamplified pulse to the counting area.

The cyclotron is operated in a somewhat special way to obtain the single short burst of neutrons. Initially, this single pulse was obtained more or less by intuition and accident. The conclusion after half a dozen runs involving successful single-pulse settings is that the parameters are interdependent in rather complicated ways. A group of settings which reproduces the single pulse (that is, from run to run) is given in Table 3.

Table 3

Settings of Cyclotron Controls for Single Pulse Operation

Indicated Radius	87.3	inches
Actual Radius	83.8	inches
Rotor Speed	680	rpm
Electric Deflector, Entrance	57	
Electric Deflector, Exit	63	
Electric Deflector, East-west	63	
Dee KV	8.8	
Dee Bias KV	2.3	
Oscillator Bias KV	0.67	
Electric Deflector KV	7.25	
Arc Tank Position	---	"Normal"
Electric Deflector Pulse Timing	95	
Arc Pulse Timing	385	
Arc Pulse KV	1.6	
Tank Filament Amperes	9.2	
Arc Pulse Width	125	
Arc Pulse Current	40	ma
Magnetic Shunts	6 1/2	
Magnetic Field Amperes	1508	amperes
Gas Flow, Meter Units	220	
Synchronizer Setting	5.0	

In this section it would be appropriate to describe an addition to the usual cyclotron controls, which has been a considerable help in obtaining single-pulse performance. This is a "synchronizer" which triggers the deflector voltage at a constant phase with respect to the rf accelerating potential. What the circuit accomplishes physically can be visualized by supposing that the cyclotron is marked off in degrees, starting with zero at any arbitrary position. The azimuthal angle of the deuteron bunch is correlated with the phase of the rf accelerating potential. If the electric deflector circuit is energized in each modulation cycle whenever deuterons pass the zero marker, say, such deuterons will be deflected in a certain characteristic manner. But if the electric deflector circuit is energized whenever deuterons pass the 73-degree marker, to specify another angle, these deuterons will be deflected in some other characteristic manner. The optimum angle is determined by test: one varies the angle at which the synchronizer triggers the deflector circuit and observes the result.

Thus the electronic synchronizer circuit produces two important results: it allows one to select the angular position of the deuteron in its orbit when the electric deflector is energized, and it ensures that subsequent deflections will occur in the same characteristic manner.

The synchronizer was developed by Don Paxon, and has performed so well that it has been incorporated in the regular cyclotron control set-up for use by experimenters who want a stabilized deflected beam.

The single pulse as seen the oscilloscope has a width at the base of about 3×10^{-8} second, but it appears from other evidence that this width is due mainly to broadening by transmission and amplification. According to measurement of the gamma distribution in time, which is the best indication of the probe pulse width, the full width at half maximum is 7×10^{-9} seconds. (See Section III E).

The probe pulse was observed on a monitor scope throughout the run. This scope was triggered by the electric deflector triggering circuit so that the pulse appeared stationary, and could be examined during the run for signs of a second pulse, if any.

D. Neutron Energy Spectrum

The as-measured spectrum of the neutrons obtained by the present time-of-flight instrumentation is shown in Figs. 7, 8, 9, and 10 for carbon, lead, bismuth, and uranium respectively. Actual number of counts per channel one shake wide is plotted versus time-of-flight in shakes.

The histograms of Figs. 7 and 8 for carbon and lead can be multiplied by $e^{\ell/\lambda}$, to remove the effect of the scatterer, the values of ℓ/λ being obtained from published cross section data versus energy.

The variation of detector efficiency with energy must next be included. The variation in detector efficiency with energy has been assumed to be proportional to the n-p total cross section. The reason for this assumption is the fact that the signal circuit bias was sufficiently low to allow detection of gamma rays from the probe. The energy of these rays was roughly measured by their absorption in carbon, magnesium, copper, and lead, as given in Table 4. From these data one calculates the photon energy to be about 5 to 10 Mev at most. Because the signal pulses from the photons could have been half as great, and still be counted, an estimate of 5 Mev seems justified as the value of bias cut-off. The lowest neutron energy being measured was about 40 Mev, so the 5 Mev energy corresponds to a point sufficiently low on the n-p differential cross section curve to justify using the total n-p cross section as an approximation.

The direct-beam neutron spectrum obtained for lead after taking into account the $e^{\ell/\lambda}$ factor and the variation of detector efficiency with energy is shown in Fig. 11 plotted against time.

Table 4

Attenuation of Gamma Rays

Element	Amount (Inches)	Counts in 2 Minutes Run 1	Run 2	Average
Direct Beam	-	106	123	115
Carbon	9	38	42	40
Magnesium	5	68	53	60
Copper	1	48	57	52
Lead	1	23	31	27

No correction has been made for the effect of the copper in the probe in attenuating the neutron beam, nor for the steel in the tank, nor air scattering in the flight path, because a detailed study of the neutron beam spectrum is incidental to this investigation. Such a study is planned as a subsequent investigation, and will include various materials as probes. One can convert Fig. 11 into an energy histogram by numerical integration, with the result shown in Fig. 12.

E. Time-of-Flight Calibration

As mentioned in the preceding section, the oscilloscope sweep is calibrated by use of a 50 MC sine wave. The projected image of the sweep in the viewer (Eastman Kodak Recordak Model No. 74MPE) can be read, if one is very careful, with an accuracy of 10^{-9} seconds, for the sweep speed employed. Using the oscillator sine wave, one divides the sweep distance as projected in the viewer into pieces of slightly-varying length, such that each represents a time increment of one shake.

The sine wave oscillator which was used was a Tektronix Mark 180 signal generator. It was adjusted in thermal equilibrium by comparison with a laboratory standard, which in turn had been checked against radio wtation WWV. The frequency of the Mark 180 was 50 megacycles within 0.001 percent.

Calibration of the delays in the probe and signal lines, as well as in the 1P21 phototube, was accomplished by use of the gamma rays from the probe. Assuming that the velocity of the gamma ray photons is $c = 2.9978 \times 10^{10}$ cm/second (the index of refraction for air is 1.00029), one may obtain the velocity of a neutron as follows (see Fig. 13):

$$D_p = D_s + (T\ O\ F)_{\gamma_4} + \chi_{p\gamma}$$

$$D_p = D_s + (T\ O\ F)_n + \chi$$

$$(T\ O\ F)_n = (T\ O\ F)_\gamma + \chi_{p\gamma} - \chi$$

$$(T\ O\ F)_n = 53.9 - \chi \qquad (2)$$

The time of flight of the gamma ray photon is obtained of course by dividing the distance of the detector from the probe (43.7 meters) by the velocity of light. The result is 14.6 shakes. The average separation of the probe pulse and the signal pulse due to photons was 39.3 shakes. These are the values which were used in obtaining Eq. 2 above.

The variation of the time separation of the gamma ray photons followed an approximately gaussian-shaped distribution. Seventy-six photons comprised the sample; all of them fell within a one-shake interval. A conservative estimate of the full width at half-maximum is 0.7 shake, corresponding to a probable error of 0.2 shake.

F. Energy Resolution and Effective Channel Energy

The limiting energy resolution arises from the variation of the time separation between the probe pulse and the signal pulse due to detection of a gamma ray photon, which as just mentioned in the previous section, followed a gaussian-shaped distribution having a standard deviation of 0.3 shake. The break in the probe pulse and signal pulse, as viewed in the projector, can be read reproducibly to 0.1 shake, if care is taken.

In the literature as well as in other theses the term "time resolution" has various interpretations. As used here it will be defined as the full base of the triangle which approximates the actual time distribution of gamma ray photons. For a probable error of the gaussian distribution of 0.2 shake, the corresponding standard deviation is 0.3 shake, the half-width at half maximum is 0.35 shake, and the full-width at half maximum is 0.7 shake. Hence, the base of the equivalent triangle is 1.4 shakes. For the flight distance of 43.7 meters, this leads to a time-resolution (per meter) of 3×10^{-10} seconds/meter.

It is to be noted that the time-resolution includes the effects of deuteron burst-duration upon striking the probe, all electronics jitters in the phototube, amplifiers and oscilloscope, as well as observer errors in film reading. Seventy-six photons comprised the sample, all of which fell within a one-shake interval. The width of the probe pulse as seen on the oscilloscope is about 3 shakes at the base, but it appears that most of this width is due to broadening by the coaxial cable and amplifiers.

From the standpoint of the phase-stable bunching of charged particles in synchrocyclotron orbits, one would expect a deuteron probe pulse of about 3 shakes duration. However, the deuterons were deflected through a region of non-constant magnetic field, which may have had a "sharpening" effect; this, plus the fact that the probe was only 1/16 inch thick radially (insulation and shielding may have added about another 1/16 inch of material), may account for the considerably shorter deuteron burst.

Using the probable error of 0.2 shake for the time uncertainty, one calculates the corresponding energy probable error for the flight distance of 43.7 meters, given in Table 2 for various energies. The derivation of the relativistic expression for energy resolution is given in the Appendix.

Because of counting statistics, the above energy resolutions could not be quoted as the uncertainty. For reasons to be discussed in Section VII, energy channels had to be employed which varied from 8 Mev to 31 Mev in width. The shape of the portion of the neutron spectrum in each of these channel-groups varies considerably, and none resembles a gaussian in the least, so the effective energy resolution is a matter of more or less arbitrary definition.

We define energy resolution in terms of an "equivalent probable error." Using the Law of Propagation of Errors we combine the 0.2 shake discussed in the preceding paragraph with one-fourth of the width in shakes of the channel group being considered. Dividing

the result by 0.6745, we obtain the "equivalent standard deviation." The energy increment which this "equivalent standard deviation" represents is defined as the standard deviation in energy, at the "effective energy" of the channel group.

The "effective energy" for a channel is defined as the energy corresponding to the centroid of the portion of the neutron spectrum included in the channel. Let N_j represent the number of observed counts in the shake-channel j. Let E_j be the energy of the shake-channel, taken at the high-energy side. The effective energy for a composite channel consisting of m shake-channels is:

$$E_{eff} = \sum_{j-1}^{j+m} N_i E_i \Big/ \sum_{j-1}^{j+m} N_i \qquad (3)$$

In the actual calculations the equivalent of the above relation on a time-of-flight basis was employed:

$$T_{eff} = \sum_{j-1}^{j+m} N_i T_i \Big/ \sum_{j-1}^{j+m} N_i \qquad (4)$$

and the energy corresponding to T_{eff} was calculated, using Eq. 2.

G. Rate of Taking Data (Avoidance of "Pile-ups")

This section is a discussion of the maximum rate of taking data. One must consider this limitation carefully or risk considerable error.

The single burst of neutrons occurs once each modulation cycle, or approximately 60 burst per second. The shape of the spectrum is such that nearly all the neutrons arrive at the scintillator within 10 shakes at the distance of 43.7 meters. The width of the pulse from the scintillator as seen on the scope is about 3 shakes; at the mode of the neutron spectrum about 40 percent of the neutrons arrive in

a three-shake interval. From a statistical consideration it is obvious that if one the average 60 neutrons were detected per second (one per burst), there would be many bursts when two neutrons would activate the scintillator within a time interval of three shakes. The person reading the film might miss the second neutron altogether; at best he might correctly interpret the result as being due to two neutrons by the size and shape of the resultant pulse, but would have to guess at the location of the "break" for the second neutron pulse.

To be on the safe side, therefore, the size of the stilbene crystal is selected so that the average counting rate is one neutron in about 20 bursts, or about 3 counts per second, as a maximum. This is the reason why the small crystal was used (one cm x 0.5 cm x 1.5 cm long).

Only the first signal pulse on each sweep is tabulated in film reading, and the usual dead-time correction is made. (See Section VI C).

IV EXPERIMENTAL PROCEDURE

The experimental procedure consisted of adjusting the cyclotron controls to obtain a single pulse of neutrons, a job that took about six to eight hours on the average. Any given parameter was set not at the value which would give a maximum pulse (flux of neutrons was not limiting at all), but at the value such that if it drifted during the running time it would still be in the single-pulse region.

Four attenuator materials (carbon, lead, bismuth, and uranium) were used, described in the next section. At 90 Mev each represented about two mean free paths of scatterer, so that the counting rate would be nearly the same for each. The scatterers were mounted on a table equipped with wheels which ran on a track, and could be pushed into the beam manually without turning off the cyclotron. Index lines insured proper line-up of the scatterers.

Each scatterer was in the beam for four minutes; the sequence bismuth, lead, carbon, uranium was always followed. All of the data for a given sequence were taken on a single 100-foot reel, to insure that if the film dimensions were affected by processing, all scatterers would be influenced in the same way. The film reels were changed at the end of the uranium data. Actual running time for each element was noted, and marks were placed on the film to separate the data. At the beginning of each reel about six feet were exposed with 50 MC sine waves.

All probe line and signal line delays and amplification were constant during the run.

V ATTENUATOR MATERIALS

The carbon, bismuth, and lead (ordinary isotopic constitution) were furnished by the metals section of the Radiation Laboratory. It was not considered necessary to check the chemical purity of the substances. The materials were weighed and measured with what is believed to be an accuracy of 99.9 percent. The data is given in Table 5 below.

The uranium was furnished by Dr. Walter Crandall's group, and consisted of machined bars about 8.6 cm x 8.6 cm x 30.5 cm long. Three bars were piled up to comprise the scatterer; the middle bar was displaced vertically by 1/4 inch, so that the edges would not be in line. Because the ends of the bars were somewhat rough the density of most of them could not be measured directly. A value of density was obtained by selecting a smooth bar. It was assumed that the variation indensity from bar to bar would be small, and would be sufficiently cancelled by the effect of three bars. The dimension in the direction of the beam was measured with micrometer calipers.

Table 5

Attenuator Materials

Element	Weight Grams	Dimensions Length* In.	Width In.	Width In.	Volume $Cm.^3$	Atoms per Sq. Cm. $\times 10^{24}$	Density ($Gm./cm^3$) Measured	Hndbk.
Carbon	26,949	26.995	6.000	6.000	15,917	5.82	1.69	2.25
Lead	58,650	7.500	6.500	6.500	5,193	0.625	11.3	11.0
Bismuth	54,484	6.962	6.997	6.998	5,556	0.499	9.80	9.67
Uranium	4,793**	1.136	12.000	1.136	254.0	0.411	18.87	18.7

*In the direction of the beam

**One bar only

VI SOURCES OF ERROR

The errors to be discussed in this section include background, forward scattering, and dead-time effects. It will be seen that only the last is appreciable, but it is small enough so that the error it introduces in a cross section value is in every case less than the associated counting-statistics error.

What might be considered to be the final check on all errors--systematic and statistical--is afforded by the use of carbon as a scatterer. Treating data for it in exactly the same way as for the unknowns, one obtains a cross section which can be compared to the accepted values. The agreement, to be discussed in Section X, is satisfactory.

A. Background

A background run was taken for 21 minutes at the conclusion of the first day's run (cyclotron having been secured for the night). A total of 202 counts were received. Thus the background counting rate was about one count in 6 seconds. The lowest of the counting rates while taking data for a scatterer was about two countes per second, average. This rate must be multiplied by the ratio of the time per modulation cycle to the time per sweep. The time per modulation cycle is about 1/60 second, the time per sweep is 50 shakes, so the effective data counting rate is about 6×10^4 counts per second, compared to which the noise counting rate is truly negligible.

Another check on this point is the fact that the projection of the scope sweep in the Recordak allowed one to examine 40 one-shake channels for data grouping, plus "border" time of about 10 shakes. The 190 Mev cutoff came at channel 28 and photons came in channel 40. Not a single count was observed in channels 29 through 39, on all the sweeps examined.

B. Forward ("Diffraction") Scattering

Forward scattering correction of the data is based on the relations derived by E. M. McMillan and D. Sewell.[13]

$$I_D = I\,(\ell/\lambda)(K - K^2)(1 + \ell/8\lambda)$$

$$K = (1/16\pi)\, k^2 a^2\, \sigma_t\, (\chi_1^{-1} + \chi_2^{-1})^2$$

For lead and 90 Mev neutrons, with the geometry as shown in Fig. 2:

$$k = (1/\hbar)\,\sqrt{2\,M\,E} = 2.15 \times 10^{13}\ \text{cm}^{-1}$$

a = scatterer "radius" = 7.6 cm approx.

x_1 = distance probe to scatterer = 1,810 cm.

x_2 = distance scatterer to detector = 2,560 cm.

σ_t = 4.5 barns ℓ/λ = 2.96

K = 0.0021

I_D = 0.0085 I

The intensity I is represented by 1550 counts, for which I_D = 13 counts due to forward scattering. The uncertainty in I resulting from counting statistics is about 39 counts. Hence the forward scattering correction for lead at 90 Mev is not relatively large.

The value of I_D/I is energy dependent, of course, and to reduce the work of making the scattering correction, one may take the maximum value to be conservative. The maximum value for the four scatterers is:

	$I_D/I \times 10^{-3}$
Carbon	2.0
Lead	8.4
Bismuth	6.4
Uranium	6.6

The forward scattering correction is listed in column labelled N_D in Table 6.

Table 6A

Observed and Corrected Counts by Channels for Carbon

Channel	N_i* Observed Counts	$\sum_i^{30} N_i$	N_J	N_D	$N_i + N_J - N_D$ Corrected Counts	$\sqrt{N_i}$	$\frac{N_J}{\sqrt{N_i}}$
1, 2, 3	4	5513	0	0	4	2	0
4, 5, 6	11	5509	0	0	11	3	0
7, 8	7	5498	0	0	7	3	0
9	7	5491	0	0	7	3	0.
10	16	5484	0	0	16	4	0
11	27	5468	1	0	28	5	0.2
12	21	5441	1	0	22	5	0.2
13	32	5420	1	0	33	6	0.2
14	95	5388	3	0	98	10	0.3
15	89	5293	3	0	92	9	0.3
16	278	5204	8	1	285	17	0.5
17	408	4926	11	1	418	20	0.6
18	489	4518	13	1	501	22	0.6
19	892	4029	20	2	910	30	0.7
20	878	3137	16	2	892	30	0.5
21	924	2259	12	2	934	30	0.4
22	568	1335	4	2	570	24	0.2
23	334	767	1	1	334	18	0.1
24	201	433	1	0	202	14	0.1
25	103	232	0	0	103	10	0
26	70	129	0	0	70	8	0
27	37	59	0	0	37	6	0
28	20	22	0	0	20	4	0
29	2	2	0	0	2	1	0
30	0	0	0	0	0	0	0

*Symbols are defined in Section XII.

Table 6B

Observed and Corrected Counts by Channels for Lead

Channel	N_i* Observed Counts	$\sum_{i}^{30} N_i$	N_J	N_D	$N_i + N_J - N_D$ Corrected Counts	$\sqrt{N_i}$	$\frac{N_J}{\sqrt{N_i}}$
1, 2, 3	65	6739	2	1	66	8	0.3
4, 5, 6	144	6674	5	1	148	12	0.4
7, 8	112	6530	4	1	115	11	0.4
9	90	6418	3	1	92	9	0.3
10	78	6328	3	1	80	9	0.3
11	104	6250	4	1	107	10	0.4
12	100	6146	4	1	103	10	0.4
13	176	6046	6	1	181	13	0.5
14	290	5870	10	2	298	17	0.6
15	254	5580	8	2	260	16	0.5
16	487	5326	15	4	498	22	0.7
17	593	4839	16	5	604	24	0.7
18	552	4246	13	5	560	23	0.6
19	998	3694	21	8	1011	32	0.7
20	854	2696	13	7	860	29	0.5
21	797	1842	8	7	798	28	0.3
22	441	1045	3	4	440	21	0.1
23	294	604	1	2	293	17	0.1
24	133	310	0	1	132	12	0
25	97	177	0	1	96	10	0
26	30	80	0	0	30	5	0
27	36	50	0	0	36	6	0
28	14	14	0	0	14	4	0
29	0	0	0	0	0	0	0
30	0	0	0	0	0	0	0

*Symbols are defined in Section XII.

Table 6C

Observed and Corrected Counts by Channels for Bismuth

Channel	N_i* Observed Counts	$\sum_i^{30} N_i$	N_J	N_D	$N_i + N_J - N_D$ Corrected Counts	$\sqrt{N_i}$	$\frac{N_J}{\sqrt{N_i}}$
1, 2, 3	120	12,345	8	1	127	11	0.7
4, 5, 6	186	12,225	12	1	197	14	0.9
7, 8	165	12,039	11	1	175	13	0.9
9	139	11,874	9	1	147	12	0.8
10	142	11,735	9	1	150	12	0.8
11	247	11,593	16	2	161	16	1.0
12	204	11,346	13	1	216	14	0.9
13	312	11,142	19	2	329	18	1.0
14	519	10,830	31	3	547	23	1.4
15	406	10,311	23	3	426	20	1.2
16	904	9,905	49	6	947	30	1.6
17	1108	9,001	54	7	1155	33	1.6
18	1120	7,893	48	7	1161	33	1.5
19	1822	6,773	69	12	1879	43	1.6
20	1579	4,951	43	10	1612	40	1.1
21	1517	3,372	28	10	1535	39	0.7
22	828	1,855	8	5	831	29	0.3
23	462	1,027	3	3	462	21	0.1
24	233	565	1	1	233	15	0.1
25	191	332	0	1	190	14	0
26	80	141	0	1	79	9	0
27	40	61	0	0	40	6	0
28	20	21	0	0	20	4	0
29	1	1	0	0	1	1	0
30	0	0	0	0	0	0	0

*Symbols are defined in Section XII.

Table 6D

Observed and Corrected Counts by Channels for Uranium

Channel	N_i* Observed Counts	$\sum_{i}^{30} N_i$	N_J	N_D	$N_i + N_J - N_D$ Corrected Counts	$\sqrt{N_i}$	$\frac{N_J}{\sqrt{N_i}}$
1, 2, 3	98	14,357	8	1	105	10	0.8
4, 5, 6	280	14,259	24	2	302	17	1.4
7, 8	228	13,979	19	2	245	15	1.3
9	170	13,751	14	1	183	13	1.1
10	189	13,581	15	1	203	14	1.1
11	269	13,392	21	2	288	16	1.3
12	223	13,123	17	1	239	15	1.2
13	366	12,900	28	2	392	19	1.5
14	576	12,534	43	4	615	24	1.8
15	543	11,958	38	4	577	23	1.7
16	1139	11,415	77	8	1,208	34	2.3
17	1252	10,276	76	7	1,321	35	2.2
18	1327	9,024	71	9	1,489	36	2.0
19	2182	7,697	98	14	2,266	47	2.1
20	1847	5,515	60	12	1,895	43	1.4
21	1655	3,668	36	11	1,680	41	0.9
22	943	2,013	11	6	948	31	0.4
23	493	1,070	3	3	493	22	0.1
24	250	577	1	2	249	16	0.1
25	160	327	0	1	159	13	0
26	91	167	0	1	90	10	0
27	61	76	0	0	61	8	0
28	15	15	0	0	15	4	0
29	0	0	0	0	0	0	0
30	0	0	0	0	0	0	0

*Symbols are defined in Section XII.

C. Dead-Time Correction

Only the signal pulse which initiated the scope sweep was counted in taking data off the film. There were various reasons for this, such as increased rate of film reading, elimination of need to distinguish between electronics "ringing" and a true second pulse (amplification in the signal line was great enough to detect gamma ray photons, so some of the amplifiers were over-driven by pulses from high-energy neutrons which happened to cause recoil protons in the forward direction), loss of true second pulses by their being merged with the initiating pulse, etc.

The scope sweep as projected in the viewer was divided into 40 one-shake channels, into which the signal pulses were sorted. Because only the first pulse of each sweep was noted, the calculation of the dead-time counting loss proceeds along the way which is designated in the literature as the "non-extended" problem,[14] modified in detail but not in principle by the fact that the counts come within a short time interval following each modulation cycle. The derivation of the relation which is to be applied to the present problem is given in the Appendix. The result is:

$$N_s = \frac{n_s}{1 - \sum_{1}^{s} r_i} \qquad (5)$$

Since this correction is only a matter of tabulation, it is given in column N_J in the data tabulation of Table 6.

The effect of the dead-time correction can be seen by comparing the calculated cross section with and without the correction. Taking that energy channel for which the correction in cross section is largest:

	Mev	A	B	$\lvert A - B \rvert$	$d\sigma$	$\frac{\lvert B - A \rvert}{d\sigma}$
Carbon	45	0.937	0.943	0.006	0.046	0.13
Bismuth	78	4.78	4.74	0.04	0.10	0.4
Uranium	78	5.20	5.13	0.07	0.12	0.6

Column A is the cross section calculated without the dead-time effect. Column B is the cross section calculated with the dead-time effect. $d\sigma$ is the error in σ due to counting statistics only.

The corrections for all energy channels are given in column N_J, of Table 7.

Table 7

Comparison of Cross Sections with and without Corrections

σ = cross section from adjusted counts ($N_i + N_J - N_D$) in barns

σ' = cross section from observed counts (N_i) in barns

SD = standard deviation due to counting statistics only in barns

	Carbon		Bismuth		Uranium	
Mev	$\lvert\sigma - \sigma'\rvert$	SD	$\lvert\sigma - \sigma'\rvert$	SD	$\lvert\sigma - \sigma'\rvert$	SD
45	0.006	0.046	0.054	0.184	0.100	0.215
53	0.002	0.035	0.052	0.178	0.099	0.206
62	0.001	0.022	0.050	0.140	0.082	0.168
70	0.002	0.016	0.042	0.125	0.080	0.148
78	0.001	0.010	0.044	0.098	0.067	0.117
89	0.002	0.008	0.031	0.089	0.055	0.106
100	0.000	0.008	0.014	0.087	0.033	0.105
113	0.001	0.010	0.006	0.112	0.009	0.134
131	0.002	0.016	0.000	0.175	0.008	0.214
155	0.000	0.027	0.000	0.312	0.000	0.368

D. Line-up Check

As a check that the scatterers were properly lined up, a run was taken with a steel shaft 7 feet long and 6 inches in diameter in the position of the scatterer. To increase the counting rate, the stilbene detector which had been used throughout the experiment was replaced by a liquid scintillator viewed by RCA 5819 phototubes. The scintillator was 5 1/2 inches in diameter and 1 inch long filled with phenylcyclohexane saturated with p-terphenyl.

While the cyclotron beam was constant, the shaft was displaced sidewise, parallel to the beam, and the counting rate was observed as a function of position. The plot of counting rate vs. position showed that the center of the shaft, and therefore the scatterer, was within 1/4 inch of being in line with the beam. Because a motion of about 2 1/2 inches was needed before the counting rate began to increase appreciably, it was certain that the detector was horizontally close to the center of the "shadow" of the scatterer.

It was not convenient to move the shaft vertically. Assurance that the detector was in the center of the vertical shadow of the scatterer came from the telescopic line-up. By sighting through the collimation from inside the shielding, one placed a telescope on the beam axis. The relative sizes and positions of the detector and scatterer were observed: the detector was in the center of the scatterer, with many "detector-diameters" to spare along all the sides. Inasmuch as the horizontal position checked so well with the counting-rate test, it is quite certain that vertically the detector also was centered with respect to the scatterer shadow.

Though hardly necessary, further assurance regarding the vertical line-up is obtained from the sizes of the stilbene crystal and the liquid scintillator. The latter had its 5 1/2 inch diameter in the vertical direction, of which perhaps three inches contributed to the counting rate, whereas the stilbene crystal had at most a one-centimeter extent in the vertical direction. From the counting-rate check with the shaft the liquid scintillator obviously was in the shadow of the shaft, and therefore one would conclude that the stilbene crystal was properly lined up.

VII FILM TRANSCRIPTION

Transcription of film is the bottleneck of the present instrumentation. This section deals with the precautions taken to be sure that it would not become a stumbling block as well.

The observed data are given in Table 6. It is to be noted that all of the film reading was done by the author--not because other help was not available, but because it seemed important that the assignment of pulses to one-shake channels be done in a consistent way to avoid possibility of systematic error. All of the data were transcribed from the film before any histograms were plotted, so that there would not be any unconscious tendency to fill out valleys or round off peaks, in accordance with what one might think "looked" good. The reading consisted of lining up the break of the signal pulse on a reference line, and visually noting the channel in which the break of the probe pulse occurred. The number designating that channel was dictated into a Sound Scriber. A picture of the mat on which the film was projected is given in Fig. 14. The slope of the lines was chosen to eliminate the necessity for lateral displacement of the scope sweep image.

Two checks were made concerning the consistency of film transcription. The first consisted of marking a representative portion of the film to give about 600 counts. This portion was reread four times on separate days. The four histograms agreed in each channel to less than one-tenth of the square-root of the number of counts in that channel.

The second check consisted of dividing the data for a given element into two portions; the first portion contained about the first two-thirds of the data, the second portion contained the rest. Treating these as if they represented data for two elements, and using the same channel groupings as for the case of a bona fide cross section, one could calculate the ratio of the two portions. These ratios are given in Table 8, and are plotted against "energy" in Figs. 15 and

16, showing standard deviations due to counting statistics. The agreement of the ratios in the various channel-groupings seemed sufficiently consistent to give confidence in the accuracy of the film transcription.

Also listed in Table 6 are the adjustments to the observed data, as discussed in Section VI. These adjustments arise from corrections for forward scattering and dead-time. Noise background is negligible.

Having the adjusted data, consisting of counts per one-shake channels, one next combines channels in such a way as to strike a balance between counting statistics error and energy resolution.

Two-shake channels seemed to give sufficiently small counting errors for the last seven of the ten points total. The first point required five one-shake channels, the second and third points required three one-shake channels each. To be sure that the grouping of channels did not result in a fortuitous trend of points, another grouping was made using the same number of channels for each of the ten points, but with a shift of one shake. To illustrate, the grouping of channels 20 and 21 furnished data for the energy channel designated as 103 Mev. In the comparison grouping, channels 21 and 22 were combined to furnish data for the energy channel designated as 110 Mev.

Now having two sets of cross section points vs. energy one could see if the sets showed the same type of trend. As a matter of fact, one set showed a rather sharper dip in cross section (for both bismuth and uranium) near 60 Mev than the other. In the interests of conservatism, the set which showed the lesser dip was selected.

It is important that the cross section for carbon for either grouping be consistent with published values. This is indeed the case; the grouping which has been selected turns out to be the one for which the carbon cross section most nearly matches the published values.

Two other groupings of data were examined, but led to no conclusions differing from those obtained from the grouping selected.

Table 8

Comparison Between Reels for the Same Element

$D = N_a/N_b$ Error $= \frac{N_a}{N_b}\left[\frac{1}{N_a} + \frac{2}{N_b}\right]^{1/2}$

"Mev"	D Carbon	Error	D Lead	Error	D Bismuth	Error	D Uranium	Error
45	1.50	0.85	1.51	0.21	1.65	0.22	4.41	0.61
53	1.00	0.61	1.37	0.20	1.52	0.20	4.68	0.57
62	1.86	0.38	1.64	0.16	1.85	0.14	4.37	0.42
70	1.46	0.24	1.63	0.13	1.89	0.13	5.33	0.40
78	1.96	0.13	1.58	0.09	1.65	0.09	4.65	0.26
89	1.69	0.09	1.60	0.08	1.63	0.07	5.17	0.22
100	1.55	0.08	1.43	0.08	1.62	0.07	5.07	0.22
113	1.49	0.11	1.50	0.11	1.61	0.11	4.59	0.33
131	1.40	0.19	1.35	0.20	1.76	0.19	3.57	0.56
155	1.68	0.32	1.27	0.38	1.18	0.34	4.64	1.02
"All"	1.62	--	1.52	--	1.67	--	4.84	--

VIII CALCULATION OF CROSS SECTION AND STATISTICAL ERROR

The comparison of cross sections of bismuth and uranium with lead entails only a minor modification of the usual method of calculation.

$$I_x = I_o\, e^{-n_x \sigma_x}$$

$$I_{Pb} = I_o\, e^{-n_{Pb} \sigma_{Pb}}$$

$$n_x \sigma_x = \ell n\, I_o - \ell n\, I_x$$

$$n_{Pb} \sigma_{Pb} = \ell n\, I_o - \ell n\, I_{Pb}$$

$$\sigma_x = \frac{n_{Pb}}{n_x} \sigma_{Pb} + \frac{1}{n_x}\, \ell n\, (I_{Pb}/I_x) \qquad (6)$$

The associated error is obtained by the Law of Propagation of Errors. We assume that the error in n_{Pb} and n_x is negligibly small, so that these parameters are to be considered constants.

$$\sigma_x = \frac{n_{Pb}}{n_x}\, \sigma_{Pb} + \frac{1}{n_x}\, \ell n\, (I_{Pb}/I_x)$$

$$(\delta\sigma_x)^2 = \left(\frac{\partial \sigma_x}{\partial \sigma_{Pb}}\right)^2 (\delta\sigma_{Pb})^2 + \left(\frac{\partial \sigma_x}{\partial I_{Pb}}\right)^2 (\delta I_{Pb})^2 + \left(\frac{\partial \sigma_x}{\partial I_x}\right)^2 (\delta I_x)^2$$

$$= (n_{Pb}/n_x)^2 (\delta\sigma_{Pb})^2 + \left(\frac{1}{n_x I_{Pb}}\right)^2 (\delta I_{Pb})^2 + \left(\frac{1}{n_x I_x}\right)^2 (\delta I_x)^2$$

$$\delta\sigma_x = (1/n_x)\left[(n_{Pb}\delta\sigma_{Pb})^2 + 1/N_{Pb} + 1/N_x\right]^{1/2} \qquad (7)$$

As already mentioned in the previous section, the grouping of one-shake channels into energy channels was made so as to obtain a balance between counting-statistics error and energy resolution. The value of the lead cross section was taken from a curve fitted by eye to the Harwell data (see Fig. 17), and a constant error of 0.05 barn was taken to apply to each point. Fitting a least-squares curve to the Harwell data did not seem to be necessary, in view of the statistical errors finally obtained, as well as for the reason next to be mentioned.

Direct comparison of bismuth and uranium with lead, which is the primary purpose of this research, can be accomplished by assigning a constant cross section to lead, say 4.5 barns. If bismuth should have exactly the same variation of cross section with energy as lead does, the experimentally determined cross section should also turn out to be a constant, except for statistical errors. In this case of assigning a constant cross section to lead, one does not obtain the absolute value of the bismuth cross section, and therefore only counting statistics are involved in the error (not the error associated with the lead absolute cross section). The result of such a calculation is given in Fig. 18 for bismuth.

A similar curve which compares uranium directly with lead is given in Fig. 19.

IX ESTIMATE OF SYSTEMATIC ERRORS

No beam monitor was used uring the run, for various reasons. One reason is that a variation in intensity would not affect the variation in cross section at all (it would simply be represented by a constant to be added to all cross section values). Another reason is that interchanging scatterers every four minutes tended to cancel the effects of beam changes, if present. Perhaps the most important reason is that it was noted in previous runs that the sizes of the individual probe pulses varied as much as 2:1, and presumably so would the neutron intensity in such bursts. To avoid having too great a dead-time correction, the size of the stilbene detector wasmade small enough so as to count one neutron in about twenty bursts (the ratio actually turned out to be 1:32, 1:26, 1:15, and 1:12 respectively, for carbon, lead, bismuth and uranium). A beam monitor would be limited by the fact that its maximum counting rate would have to be less than one neutron per burst. The question would remain whether the monitor, in its sampling of bursts, would be really representative of those bursts which the detector was sampling.

To make an estimate of the error in the absolute value of the cross sections obtained by assuming that the beam was constant, one can compare the cross section for carbon with the published values. The curve fitted by eye to points obtained in this investigation differed by about 1 percent from the curve fitted by eye to published values. This would suggest that the absolute value of the cross sections obtained for bismuth and uranium might have a systematic error of one percent also. To be conservative, one might increase this estimate of the systematic error to 5 percent, leading to a value of $\pm$ 0.2 barn as the estimate of the systematic error in the absolute values of the bismuth and uranium cross section.

The energy scale was calibrated by the time of flight of gamma rays, as discussed in Section III E. The time of flight of a neutron or photon could be measured with a probable error of 0.2

shake, which includes the effect of neutron production time (deuteron probe burst), jitter in phototube and electronics, and film reading uncertainty. This leads to a time resolution per meter of 3×10^{-10} seconds per meter, at the distance of 43.7 meters.

The distance of 43.7 meters is uncertain to 0.3 meter at most (scaling off distances inside cyclotron from drawing), and film reading is uncertain to 0.1 shake, with care being taken. The uncertainty in absolute time-of-flight is thus about 0.2 shake, so at 90 Mev the absolute value of quoted energy seems not to be in error by more than 1.2 Mev. To be conservative, one might quote a figure of ± 2 Mev at 90 Mev as the estimate of absolute energy scale error, or, in time units, 5×10^{-10} seconds/meter error in absolute time of flight.*

X RESULTS AND DISCUSSION

The variation of neutron total cross section with energy for bismuth and uranium is given in Table 9 and in Figs. 20 and 21 respectively. Comparison with a curve drawn by eye for Taylor and Wood's lead results is shown in Fig. 17. Results obtained in this research for the carbon neutron total cross section (intended to serve as a check on the instrumentation) is given in the same table and in Fig. 22, where published values are also shown. A smooth curve has been fitted by eye to the published values to facilitate comparison.

Variation of the cross section for bismuth and uranium relative to lead is given in Table 10 and in Figs. 18 and 19. These results were obtained by taking a constant value of 4.50 barns for the lead cross section.

Considering the results of Fig. 18 first, it seems that bismuth has, within the statistical error, the same variation of cross section with energy as does lead, from 70 to 160 Mev. Two points at 45 and 53 Mev seem to lie about two standard deviations above the lead value. If significant, these values would suggest that bismuth has a sharper rise in cross section on the low-energy side of the lead dip in cross section.

Turning to Fig. 19, one sees that all of the values for the uranium cross section lie above the lead value, which had been taken constant at 4.50 barns. If one draws a reference line (shown dotted) at 4.90 barns, it is seen that only two of the points are as much as two standard deviations away. This shows that uranium has the same variation in cross section with energy as does lead, within the statistical error. Also, to the extent that the value of 4.50 barns represents the average value of the lead cross section, the value of 4.90 barns represents the average value of the uranium cross section, for the entire 90 Mev neutron spectrum. The values quoted by DeJuren and Knable for "95 Mev" neutrons are 4.48 barns for lead and 4.92 barns for uranium. The agreement seems to be satisfactory.

Table 9

Cross Section and Energy for Carbon, Bismuth, and Uranium

All cross sections are in barns

All errors are in standard deviations

Neutron Mev Effective	Error* Mev	Channel Width Mev	Channels	Carbon σ	Carbon Error	Bismuth σ	Bismuth Error	Uranium σ	Uranium Error
45	3.8	9.5	3, 4, 5, 6, 7	0.943	0.046	4.74	0.18	4.96	0.21
53	3.0	7.5	8, 9, 10	0.825	0.035	4.50	0.18	4.44	0.21
62	3.8	8.5	11, 12, 13	0.742	0.022	4.14	0.14	4.53	0.17
70	3.2	7.5	14, 15	0.698	0.016	4.92	0.12	5.30	0.15
78	3.8	9.5	16, 17	0.590	0.010	4.74	0.10	5.13	0.12
89	4.6	11.5	18, 19	0.531	0.008	4.71	0.09	5.10	0.11
100	5.5	13.5	20, 21	0.476	0.008	4.54	0.09	5.00	0.11
113	6.5	17.5	22, 23	0.418	0.010	4.22	0.11	4.67	0.13
131	8.4	22.0	24, 25	0.363	0.016	3.63	0.17	4.29	0.21
155	11.0	30.0	26, 27	0.271	0.027	3.02	0.31	2.90	0.37

*See discussion in Section III F.

Table 10

Cross Sections Referred to Lead

(Lead σ = 4.50 at all energies)

Cross sections are given in barns

All errors are in standard deviations

Neutron Mev Effective	Error* Mev	Channel Width Mev	Channels	Bismuth σ_{rel}	Bismuth Error	Uranium σ_{rel}	Uranium Error
45	3.8	9.5	3, 4, 5 6, 7	4.96	0.17	5.26	0.20
53	3.0	7.5	8, 9, 10	4.90	0.17	4.95	0.19
62	3.8	8.5	11, 12, 13	4.32	0.13	4.76	0.15
70	3.2	7.5	14, 15	4.65	0.11	4.99	0.13
78	3.8	9.5	16, 17	4.48	0.08	4.81	0.09
89	4.6	11.5	18, 19	4.43	0.06	4.76	0.07
100	5.5	13.5	20, 21	4.46	0.06	4.92	0.07
113	6.5	17.5	22, 23	4.59	0.09	5.12	0.11
131	8.4	22.0	24, 25	4.49	0.16	5.35	0.20
155	11.0	30.0	26, 27	4.52	0.31	4.78	0.36

*See discussion in Section III F.

It remains to be seen whether the statistical error is sufficiently small to reveal variations in cross section. Referring now to Fig. 20 for bismuth, one sees that the points at 62 and 70 Mev are separated by 0.78 barn. The errors in standard deviations (which include the uncertainty in lead cross section as well as counting uncertainty) are 0.14 and 0.12 barns respectively. The difference in cross section is thus 5.6 times as great as the larger standard deviation, which may indeed by considered a significant amount. The trend of points seems to show a dip in cross section at about 63 Mev.

The results for uranium, as shown on Fig. 21, also seem to show a dip in cross section at about 55 to 60 Mev. The difference in cross section between points at 62 and 70 Mev is 0.77 barn. The corrseponding uncertainties in cross section are 0.17 and 0.15 barn. The difference in cross section is 4.5 times as great as the larger standard deviation, and this may be considered significant. The trend of points seems to leave no doubt that a definite dip is present.

The variation of carbon cross section, as obtained in this experiment, agrees well with published values.[6,15] The results are given in Fig. 22. It will be recalled that no constants have been added to the cross section or energy scales. The agreement therefore seems to be conclusive proof that the time-of-flight equipment had no great systematic error.

The importance of the agreement of carbon cross section with results obtained elsewhere stems from the fact that time-of-flight technique in this energy region is extremely sensitive to systematic errors of the order to one shake. If for example, a shift of one shake were to take place in the lead time-spectrum, a completely artificial "dip" or "rise" would result in the cross sections obtained for the other elements.

The single-pulse operation of the cyclotron, in view of all the interdependent variables which might drift over a period of two days, had to be checked regularly during the runs. A monitor scope, triggered by the electric deflector circuit, showed a single

pulse of deuterons to be striking the probe. However, if other material were present (such as the probe support base plate, etc.), those deuterons which missed the probe might strike the other material after a revolution, and give a second pulse of neutrons which would make the spectrum hopelessly garbled. Such an occurrence--which in fact did happen during the March 15, 1953 run--could not be seen on the monitor scope. It is necessary to examine the neutron spectrum itself, to see if spurious pulses are in evidence. They would show up as modes displaced 10 shakes from the main mode (ten shakes represents the period of a 195 Mev deuteron in the 15,000 gauss magnetic field). The spectra given in Figs. 7, 8, 9, and 10 for carbon, lead, bismuth, and uranium show no signs of second pulses anywhere, which assures one that single-pulse operation had been achieved.

(It might be remarked at this point that spurious pulses, not seen on the monitor scope because they originate from material other than the probe being struck by deuterons, could be resolved from statistical fluctuations on the time-spectrum only after much film transcription, long after the run had been concluded.)

Another check on the reliability of the instrumentation is furnished by Fig. 11 which shows the "direct beam neutron spectrum" on a time-scale. The histograms of Figs. 7 and 8 for carbon and lead are multiplied by $e^{\ell/\lambda}$, to remove the effect of the scatterer, the values of ℓ/λ being obtained from published cross section data versus energy. Presuming that the direct neutron beam was constant, these spectra derived from carbon and lead data should be the same, within counting statistics. Examination of Fig. 11 shows this to be the case, which is one more assurance that the instrumentation had been free from systematic errors for these two elements, and therefore presumarly for the others as well.

The direct beam neutron spectrum, obtained from the "detected bean neutron spectrum" by including the factor taking care of variation of detector efficiency with energy is shown in Fig. 12. A study of the direct beam spectrum is not directly related to the

purpose of this investigation, and so further remarks concerning deuteron-stripping theory are placed in the Appendix. Assurance is obtained from the shape of the direct beam spectrum, however, regarding reliability of the instrumentation. No counts at all were observed above 195 Mev neutron energy. The sharpness of the spectrum, particularly the rapid drop-off on the low energy side indicate good agreement with Serber's stripping theory.

Concerning the theoretical interpretation of the cross section results, a note has been published by J. D. Lawson,[16] but it is so approximate as to be almost speculation. The argument is based on an optical analogy. The change of phase of the neutron wave is calculated for a slab of nuclear matter of thickness D, placed with its faces parallel to the wavefront. The diffraction scattering is a maximum when the phase change is an odd multiple of π, and a minimum when it is an even multiple. A phase change of $n\pi$ Lawson states is expected to occur at an energy given by

$$E = 10^{26}\ \pi^2\ b^2\ D^2/n^2$$

$$b \approx 0.6$$

$$D = 2.8 \times 10^{-13}\ A^{1/3}$$

$$A = \text{Atomic weight}$$

The value of energy he calculates for various materials for a phase change of π is given below. The maxima and minima predicted by his formula at lower energies he dismisses as not being in the region of validity of the assumptions upon which the relation is based.

Material	Energy (Mev)
Carbon	14
Aluminum	26
Copper	46
Cadmium	64
Lead	100
Bismuth	100
Uranium	109

Other theoretical calculations are in progress by members of the theoretical group at UCRL.

At the time of this writing the complementary investigation of neutron cross section of antimony and tantalum by Boris Ragent is nearly finished; when completed, it should throw additional light on the nature of the dip in cross section at high energy.

XI ACKNOWLEDGMENTS

The author wishes to express his gratitude to Prof. H. F. York for suggesting this technique, and to Prof. L. W. Alvarez, under whose guidance this work was carried out, for valuable suggestions. The help and cooperation of the author's colleague, Boris Ragent, has been of inestimable value; he must share equally in any credit for this research.

Thanks are due also to Robert Silver, Robert Donaldson, John Leahy, and George Hecht, whose help with preparations and particularly at times of runs was indeed welcome. The cooperation of James Vale, Lloyd Hauser and the cyclotron crew was of great help during the long hours spend searching for an elusive single pulse. Vern Ogren and Don Paxon both rendered expert electronics assistance in many ways, which the author has appreciated very much. Roland Michaelis also deserves a note of appreciation for patiently developing reels on reels of film.

The paper on "Operation of the 184-inch Cyclotron" by Henrich, Sewell, and Vale[17] has been consulted frequently; the data in it have contributed considerably to the development of this time-of-flight method.

XII NOMENCLATURE

Page	Symbol	Meaning
6	θ	Angle of incidence
	η	Order of diffraction
	d	Separation of planes
	λ	de Broglie wave length
	M	Mass of neutron
	h	Planck's constant
7	α	Incoming particle
	β	Outgoing particle
	σ	Cross section
	ℓ	Angular momentum in $\hbar$ units
	Γ^s	Width of level s
	Γ^s_α	Partial width of Γ^s associated with emission of α
	Γ^s_β	Partial width of Γ^s associated with emission of β
	Γ^s_{rad}	Partial width of Γ^s associated with emission of γ
	ϵ_α	Energy of incident particle, near $\epsilon_{\alpha s}$
	$\epsilon_{\alpha s}$	Resonance energy
	A^ℓ_{pot}	Potential scattering amplitude corresponding to scattering which would take place if nucleus were replaced by a perfectly reflecting sphere
8	$\bar{r}$	Vector between center of nucleus and neutron
	k	Wave number of wave outside nucleus
	η_ℓ	Complex coefficient of outgoing wave with angular momentum
	$Y_{\ell,0}$	Spherical harmonic (m = 0)
9	f_ℓ	Logarithmic derivative of wave function at nuclear boundary
	Δ_ℓ, S_ℓ	Real numbers which depend on wave number k, and radii of nucleus and neutron, and angular momentum
	ξ_ℓ	Phase constant
	$k + k_1$	Wave number of wave inside the nucleus

Page	Symbol	Meaning
10	K	Absorption coefficient
	R	Radius
	$k + k_1$	Wave number of wave inside nucleus
	A	Atomic weight
	Z	Atomic number
	V	Mean potential energy of neutron in nucleus
	E	Neutron energy
	T	Distance in nuclear matter
	a	Amplitude of wave
	ρ, s	Distances involved in geometrical calculation
16	I_o	Direct beam neutron spectrum
	F	Factor involving variation of detector efficiency with energy
	I_1	Spectrum following a scatterer
	n	Number of atoms per sq. cm.
27	D_P	All delays in probe line
	D_S	All delays in signal line (including lP2l delay)
	$\chi_{P\gamma}$	Average separation on scope sweep as projected in viewer, between probe pulse and signal pulse due to gamma photon, in shakes
	χ	Separation on scope sweep as projected in viewer, between probe pulse and signal pulse due to neutron, in shakes
36	k	$(1/\hbar)\ \sqrt{2\,M\,E}$
	a	Scatterer "radius"
	χ_1	Distance from probe to scatterer
	χ_2	Distance from scatterer to detector
	I_D	Number of neutrons diffracted into detector by scatterer during time that spectrum is observed.

Page	Symbol	Meaning
37	N_i	Observed number of counts in channel i
	N_J	Correction to observed counts due to "dead-time" effect
	N_D	Correction to observed counts due to forward scattering
42	N_s	True number of counts in channel s
	n_s	Observed number of counts in channel s
	r_i	Observed number of counts per sweep in channel i
49	I_o	Direct beam intensity
	I_x	Beam intensity after passing scatterer x
	n_x	Number of atoms of scatterer x per sq. cm.
	σ_x	Cross section in barns for scatterer x
49	$\delta\sigma_x$	Error in σ_x
	N_{Pb}	Counts for lead in channel grouping selected
	N_x	Counts for scatterer x in channel grouping selected
	$P_\perp$	Momentum component of neutron in deuteron perpendicular to motion of center of mass

XIII APPENDICES

A. Direct Beam Neutron Spectrum and Stripping Theory

The direct beam neutron spectrum has been briefly discussed in the preceding material. Here we consider the spectrum from the viewpoint of Serber's stripping theory.[12] He has derived expressions for the energy distribution for "transparent" and "opaque" nuclei as follow:

$$P(E)\,dE = \frac{\sqrt{E_d\,\epsilon}\;dE}{\pi[(E - \frac{1}{2}E_d)^2 + E_d\,\epsilon]} \qquad \text{"Transparent" (all angles)}$$

$$d\sigma = \frac{1}{4}\pi R\,R_d \frac{E_d\,\epsilon\,dE}{[(E - \frac{1}{2}E_d)^2 + E_d\,\epsilon]^{3/2}} \qquad \text{"Opaque" (All angles)}$$

The comment "all angles" refers of course to the fact that the above energy distributions are what one would expect if the neutrons from stripped deuterons were measured over the forward cone (ranging from 0° to at least 10°).

If we neglect multiple scattering for the moment, then because of the collimation, only neutrons in the forward direction are measured in what is called the "90 Mev beam." Particularly for the geometry of this experiment, only neutrons at angles of θ approximately 0.05° or less have been measured. For such forward angles, one derives, following Serber's method, the distributions:

$$P_T(E)\,dE = \frac{1}{\pi}\frac{(P_\perp)^2_{max}}{M}\frac{E_d^{3/2}\sqrt{\epsilon}\,dE}{[(E - \frac{1}{2}E_d)^2 + E_d\,\epsilon]^2} \qquad \text{"Transparent" (forward only)} \qquad (8)$$

$$P_o(E)\,dE = \frac{1}{\pi}\frac{(P_\perp)^2_{max}}{M}\frac{E_d^2\,\epsilon\,dE}{[(E - \frac{1}{2}E_d)^2 + E_d\,\epsilon]^{5/2}} \qquad \text{"Opaque" (forward only)} \qquad (9)$$

The relative sharpness of the four distributions (in terms of full width at half maximum) are given in Table 11 below, for 195 Mev deuterons.

Table 11

Relative Sharpness of the Four Distributions

Type of Nucleus and Angle of Observation	Full Width at Half Maximum In Mev
Transparent, all angles	41.0
Opaque, all angles	31.4
Transparent, forward only	26.4
Opaque, forward only	23.2

These distributions refer to "thin" targets; i.e., targets in which the deuteron loses practically no energy. The spectrum obtained in this experiment comes from a "thick" target, because it is necessary to stop the deuterons completely by ionization in order to collect a charge pulse on the probe. To obtain a theoretical expression for the energy distribution for a "thick" target one must include the deuteron-energy-dependent factors which affect yield of neutrons.

In a thick target the number of atoms encountered by a deuteron per unit energy loss dE is proportional (approximately) to the deuteron energy. This is obtained from the expression for energy loss:

$$-\frac{dE}{d\chi} \sim \frac{1}{E}$$

$$-d\chi \sim E dE$$

Because the experimental spectrum is rather sharp, one might try Eq. 9. An expression for the thick target spectrum would therefore be:

$$[P_o(E)\,dE]_{thick} \sim \int_{E_2}^{E_1} \frac{E_d^3\,dE\,dE_d}{[(E - \frac{1}{2}E_d)^2 + E_d\,\epsilon]^{5/2}} \qquad (10)$$

The spectrum obtained from this equation does not fit the experimental one at all.

Earlier in these considerations we neglected multiple scattering in the target. It may be that this is not at all justified. Calculation of the RMS scattering angle shows that it is relatively small over much of the deuteron range, but individual scatterings--which could be relative large--might introduce an "all angles" effect in the neutron distribution. If most of the deuterons are lost by being scattered out of the target while still possessing nearly their initial energy, due to plural scattering, one would not be too surprised to find a "thin" target spectrum coming from the actual "thick" target.

Figure 23 shows the experimental spectrum in histogram form with the Serber thin-target opaque-nucleus all-angles distribution plotted. The experimental spectrum has been corrected for variation of detector efficiency with energy. The cross-hatched blocks and points with errors attached are published data of Hadley[18] et al and Brueckner[19] et al.

It is to be recalled that no beam monitor is necessary in obtaining the spectrum in the present time-of-flight instrumentation, and for this reason alone the measurement may be more reliable than previous ones by other methods.

These comments are intended only to indicate that the present instrumentation seems well adapted to a study of direct beam spectra. It is intended to use the equipment to obtain spectra with different materials as targets (beryllium, copper, antimony, and lead). More detailed and precise theoretical analyses are also to be made, particularly with regard to scattering effects.

B. Calculation of "Dead-Time" Correction

Let N_S = true number of counts in channel S in time T

n_s = observed number of counts in channel S in time T

r_1 = observed number of counts in channel 1 per sweep

T = time of observation in seconds

f = number of sweeps per second (approximately 60/sec.)

η = Tf = number of sweeps in time T

R_1 = true number of counts in channel 1 per sweep

Consider channel 1:

$\frac{n_1}{T}$ = observed number of counts per second (average)

= number of sweeps per second which are "dead"

$\frac{n_1}{T}\frac{1}{f}$ = fractional number of sweeps which are "dead"

$1-\frac{n_1}{T}\frac{1}{f}$ = fractional number of sweeps which are not "dead"

Therefore $$(1 - \frac{n_1}{T}\frac{1}{f}) = 1 - r_1$$

$$(1 - r_1) R_1 = r_1$$

$$R_1 = \frac{r_1}{1 - r_1}$$

$$\therefore N_1 = \frac{n_1}{1 - r_1}$$

Using same procedure for channel S, we obtain:

$$N_S = \frac{n_s}{1 - \sum_1^s r_1} \qquad (6)$$

C. Calculation of Energy Resolution on Relativistic Basis

L = flight distance

$\beta = v/c$

m = relativistic neutron mass

m_o = neutron rest mass

$$m = m_o / \sqrt{1 - \beta^2}$$

$$dm = (m^3/m_o^2)\,\beta d\beta$$

$$\beta^2 = 1 - m_o^2/m^2$$

$$d\beta = -(L/ct^2)\,dt$$

$$dm = -(m^3/m_o^2)\left(\frac{m^2 - m_o^2}{m^2}\right)\frac{dt}{t}$$

$$\frac{dm}{m} = -\frac{m^2 - m_o^2}{m_o^2}\,\frac{dt}{t}$$

XIV REFERENCES

1. G. Breit and E. Wigner, Phys. Rev. 49, 519 (1936).
2. J. Blatt and V. Weisskopf, Theoretical Nuclear Physics, John Wiley and Sons, 1952.
3. R. Serber, Phys. Rev. 72, 1114 (1947).
4. S. Fernbach, R. Serber, and T. Taylor, Phys. Rev. 75, 1352 (1949).
5. J. DeJuren and B. Moyer, Phys. Rev. 81, 919 (1951).
6. A. Taylor and E. Wood, Phys. Rev. 87, 907 (1952).
7. A. Taylor and E. Wood, Phil. Mag. 44, 95 (1953).
8. V. F. Weisskopf, Brookhaven Conference Report, BNL224C18 (1953).
9. W. Linlor and B. Ragent, Bull. Amer. Phys. Soc. 28, 16 (1953) D2
10. B. Ragent and W. Linlor, Bull. Amer. Phys. Soc. 28, 16 (1953) D3
11. W. M. Brobeck, E. O. Lawrence, K. R. MacKenzie, E. M. McMillan, R. Serber, D. C. Sewell, K. M. Simpson, R. L. Thornton, Phys. Rev. 71, 449 (1947).
12. R. Serber, Phys. Rev. 72, 1008 (1947).
13. E. McMillan and D. Sewell, Diffraction Effect in Neutron Attenuation Measurements, MDDC 1558 (1947).
14. D. Halliday, Introductory Nuclear Physics, John Wiley and Sons (1950).
15. G. Mott, G. Guernsey, and B. Nelson, Phys. Rev. 88, 9 (1952).
16. J. D. Lawson, Phil. Mag. 44, 102 (1953).
17. L. R. Henrich, D. Sewell, and J. Vale, Rev. Sci. Inst. 20, 887 (1949).
18. J. Hadley, E. Kelley, C. Leith, E. Segre, C. Wiegand, and H. York, Phys. Rev. 75, 351 (1949).
19. K. Brueckner, W. Hartsough, E. Hayward, and W. M. Powell, Phys. Rev. 75, 555 (1949).

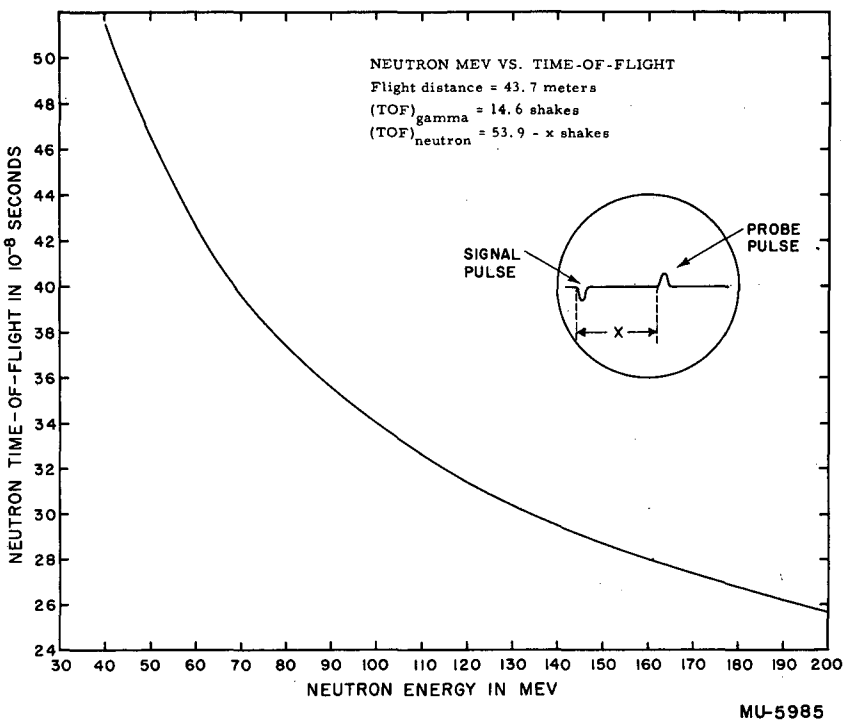

Fig. 1 Neutron energy in Mev vs. time of flight in shakes. $(TOF)_{gamma}$ = 14.6 shakes. $(TOF)_{neutron}$ = 53.9 - X shakes.

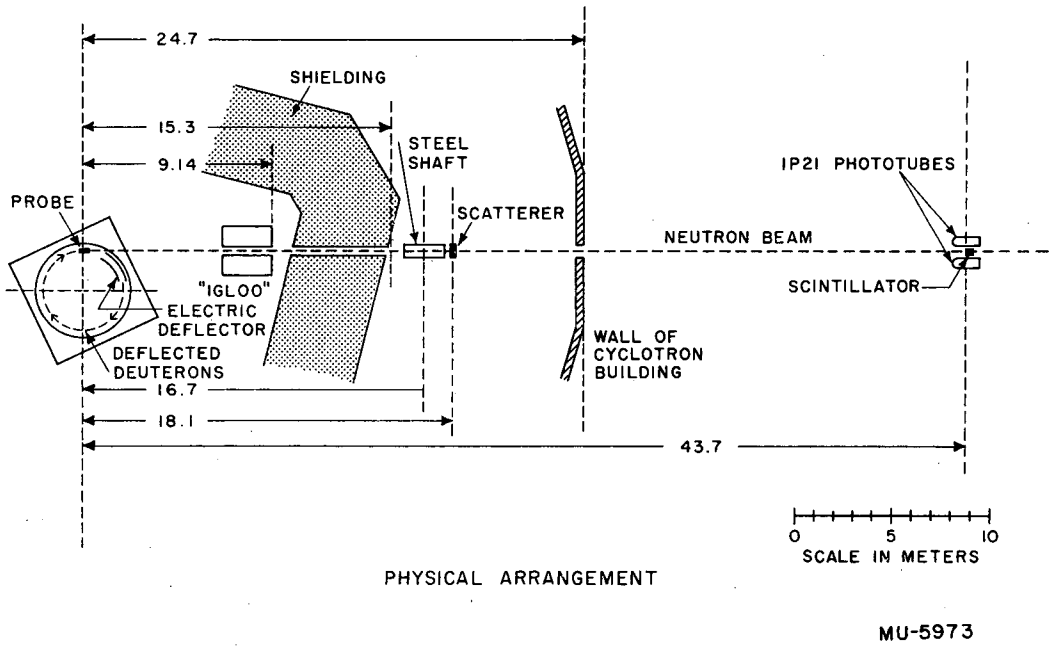

Fig. 2 Physical arrangement. Neutron beam is collimated to 3 inches x 3 inches by "igloo." Scatterers are 6 inches x 6 inches area. Steel shaft is placed in position shown when background runs are made.

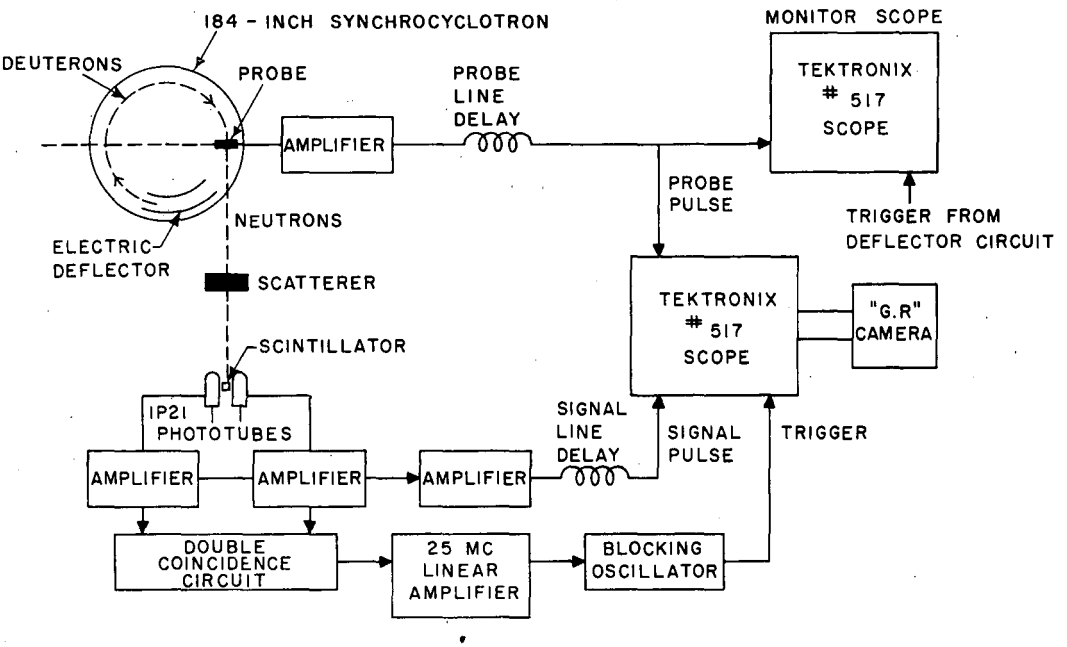

BLOCK DIAGRAM OF ELECTRONICS

MU-5975

Fig. 3 Block diagram of electronics.

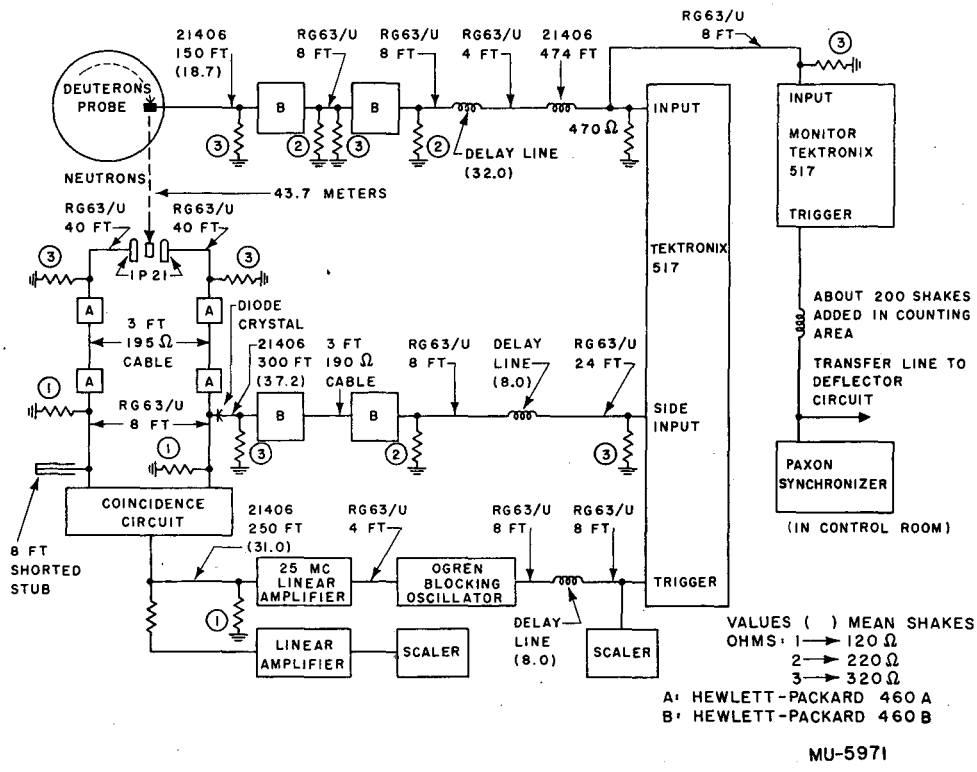

Fig. 4 Detailed diagram of electronics.

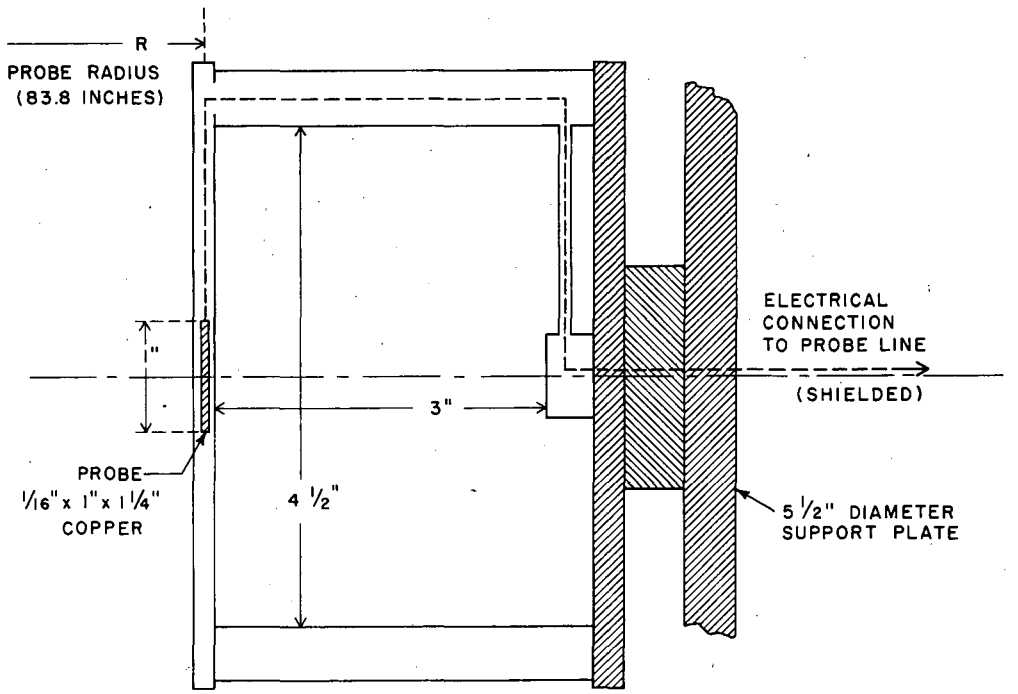

Fig. 5 Schematic drawing of probe assembly. Radial extent of 1/16 inch for copper probe is increased to about 1/4 inch by addition of insulation and shielding. (See photographs of Fig. 6).

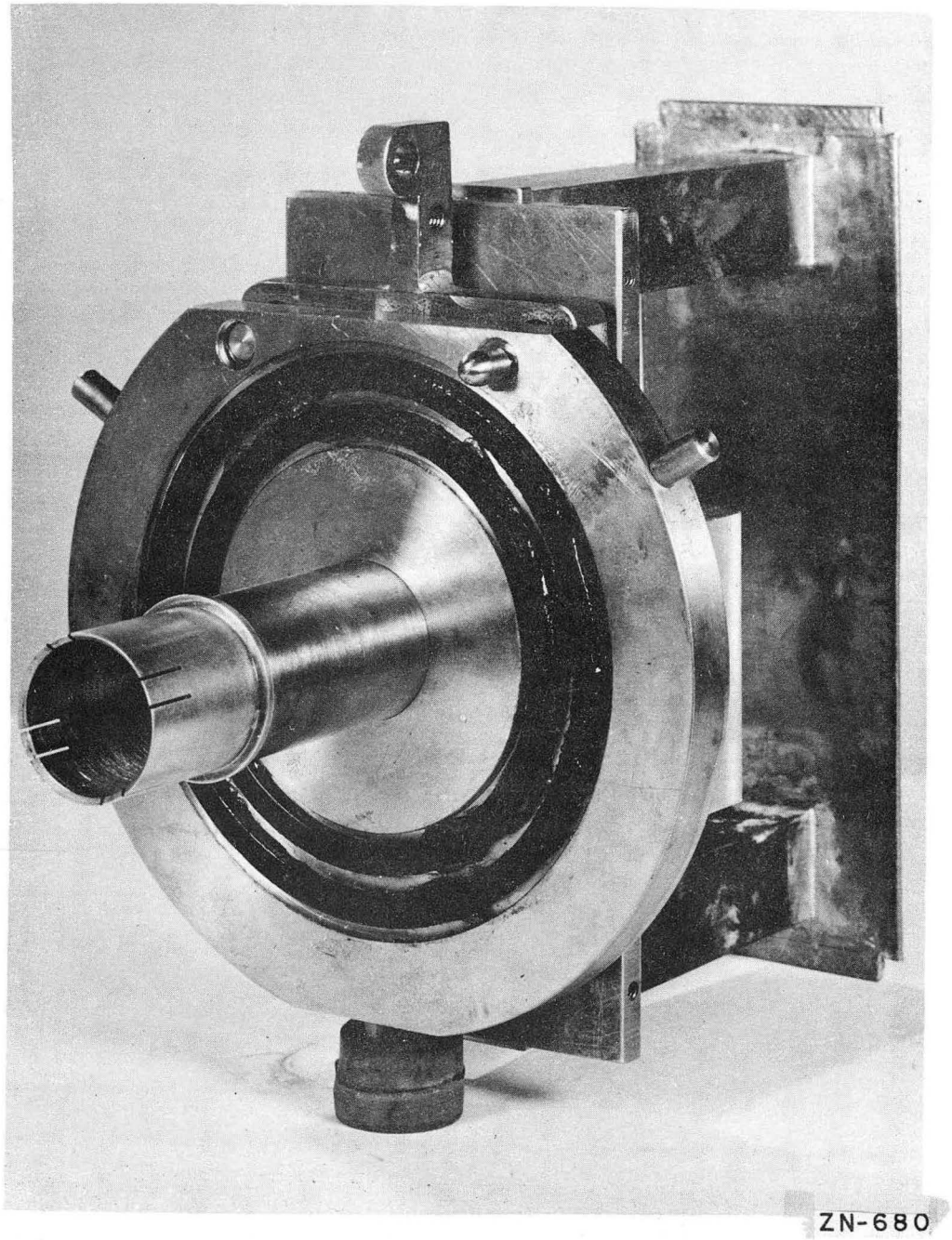

Fig. 6a Photograph of probe.

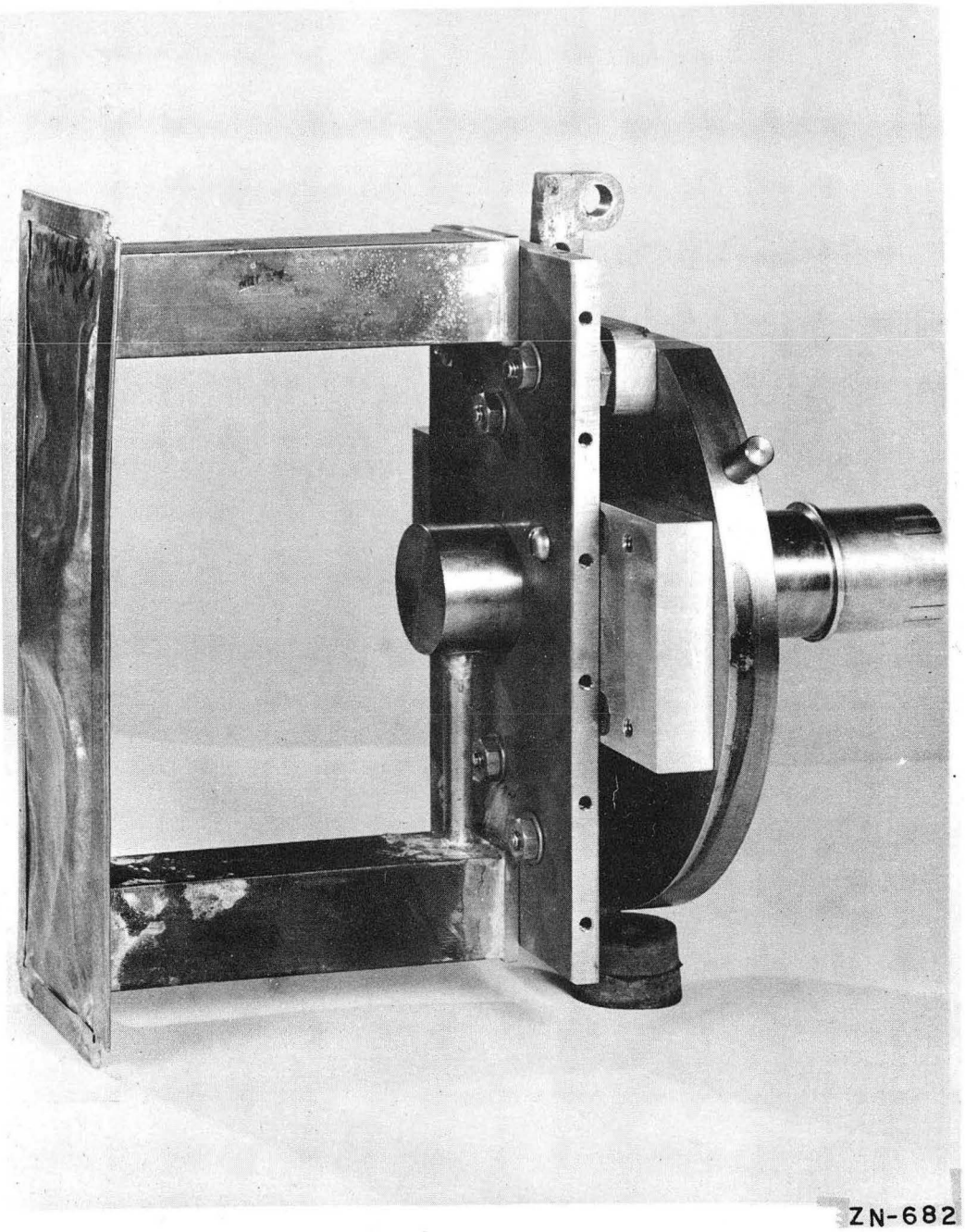

Fig. 6b Photograph of probe.

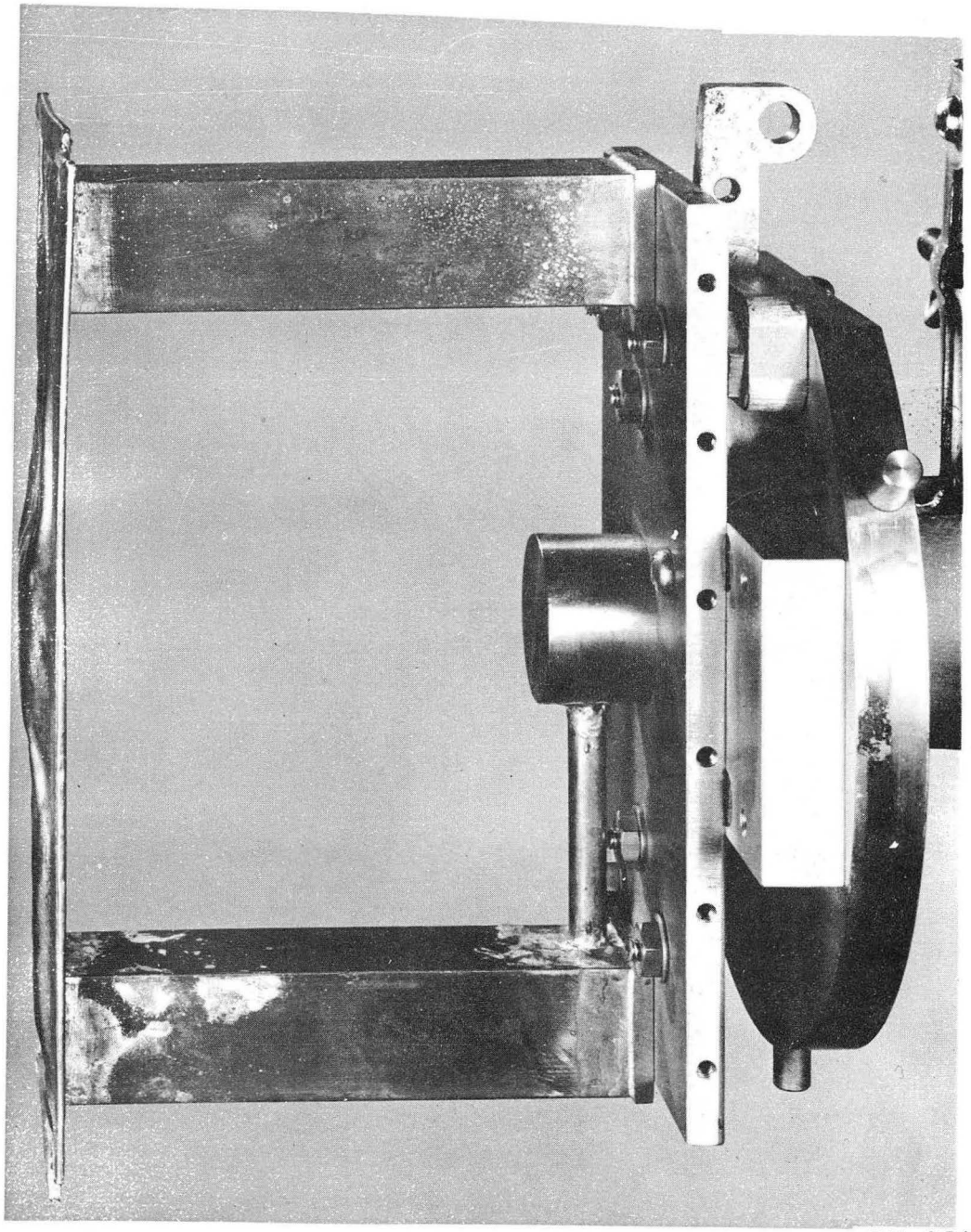

Fig. 6c Photograph of probe.

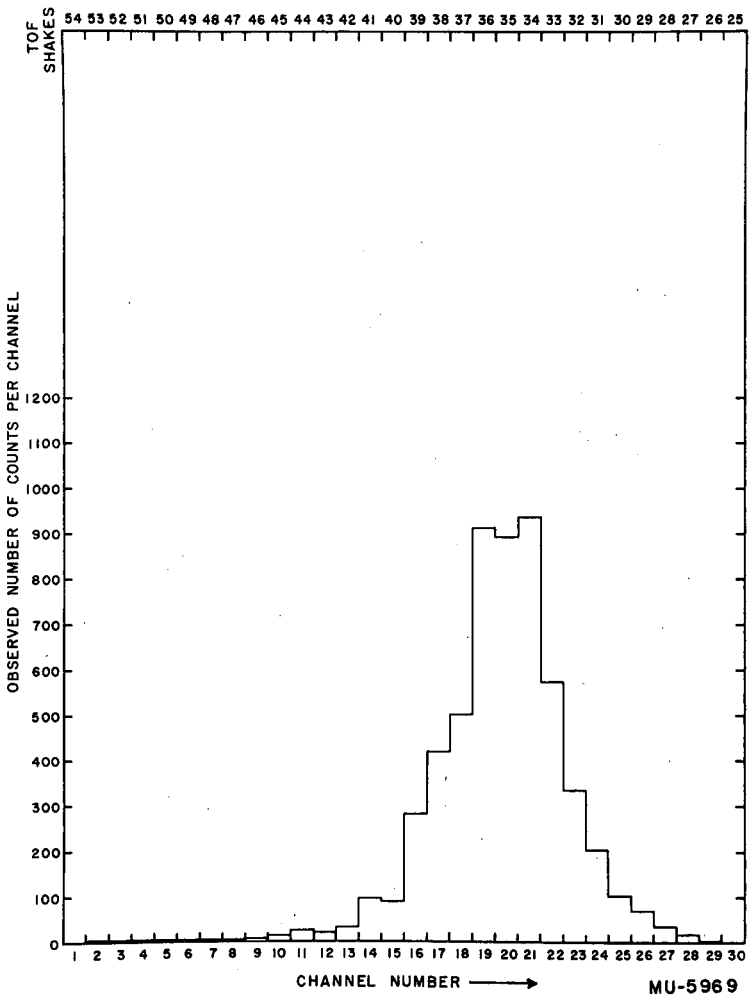

Fig. 7 Carbon neutron spectrum. Ordinate is the observed number of counts in a stilbene scintillator per channel (one shake wide), plus a "dead-time" correction amounting to a few percent. Abscissas are channel number and time of flight in shakes. Carbon atoms per sq. cm. = 5.82×10^{24}.

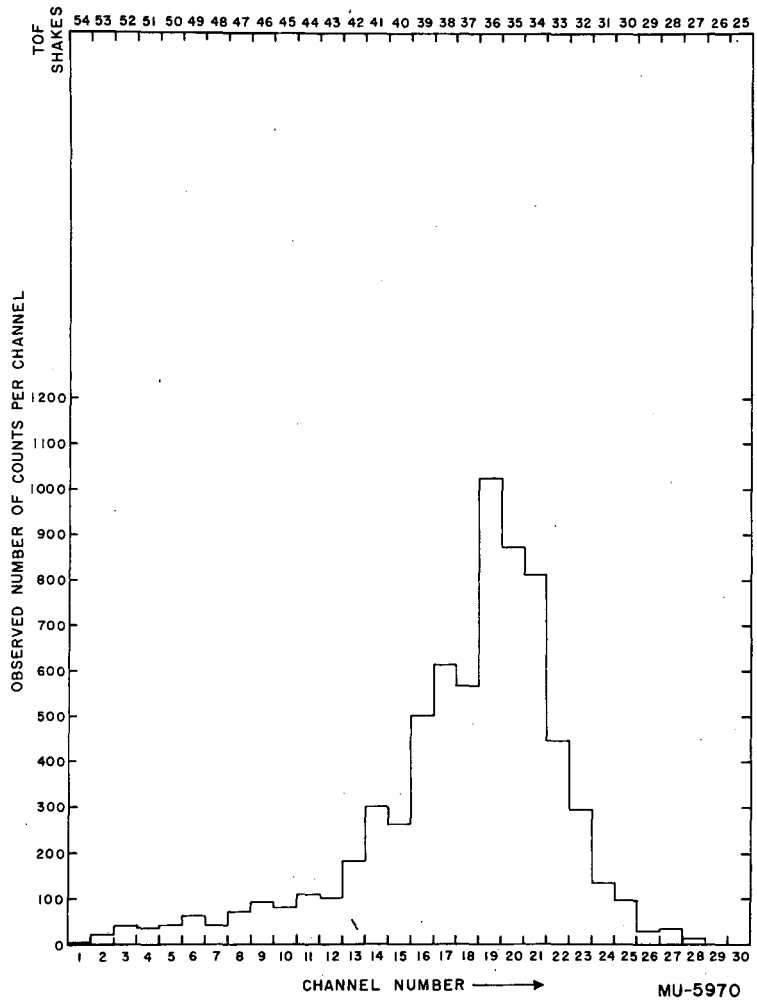

Fig. 8 Lead neutron spectrum. Ordinate is the observed number of counts in a stilbene scintillator per channel (one shake wide), plus a "dead-time" correction amounting to a few percent. Abscissas are channel number and time of flight in shakes. Lead atoms per sq. cm. = 0.625×10^{24}.

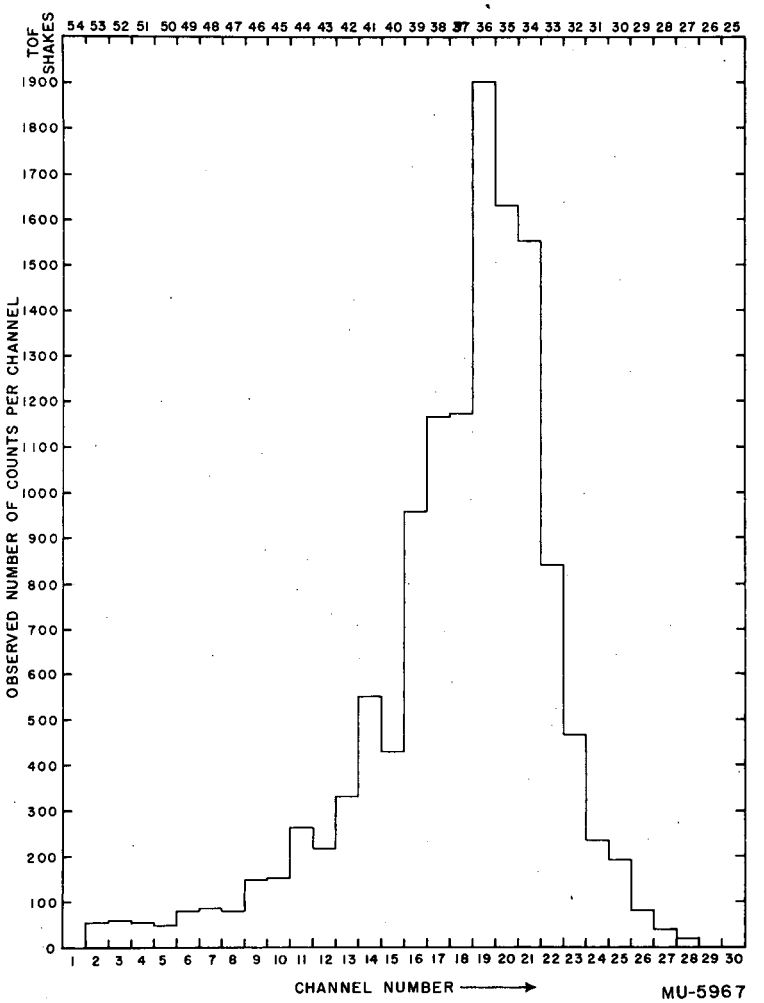

Fig. 9 Bismuth neutron spectrum. Ordinate is the observed number of counts in a stilbene scintillator per channel (one shake wide), plus a "dead-time" correction amounting to a few percent. Abscissas are channel number and time of flight in shakes. Bismuth atoms per sq. cm. = 0.499×10^{24}.

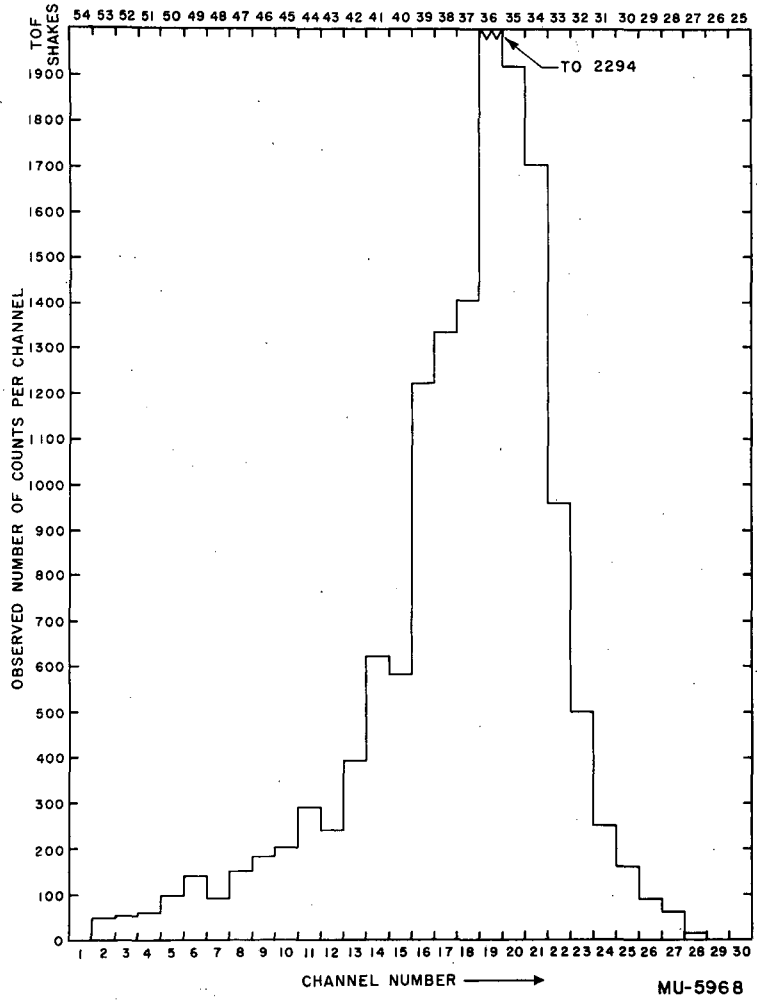

Fig. 10 Uranium neutron spectrum. Ordinate is the observed number of counts in a stilbene scintillator per channel (one shake wide), plus a "dead-time" correction amounting to a few percent. Abscissas are channel number and time of flight in shakes. Uranium atoms per sq. cm. = 0.411×10^{24}.

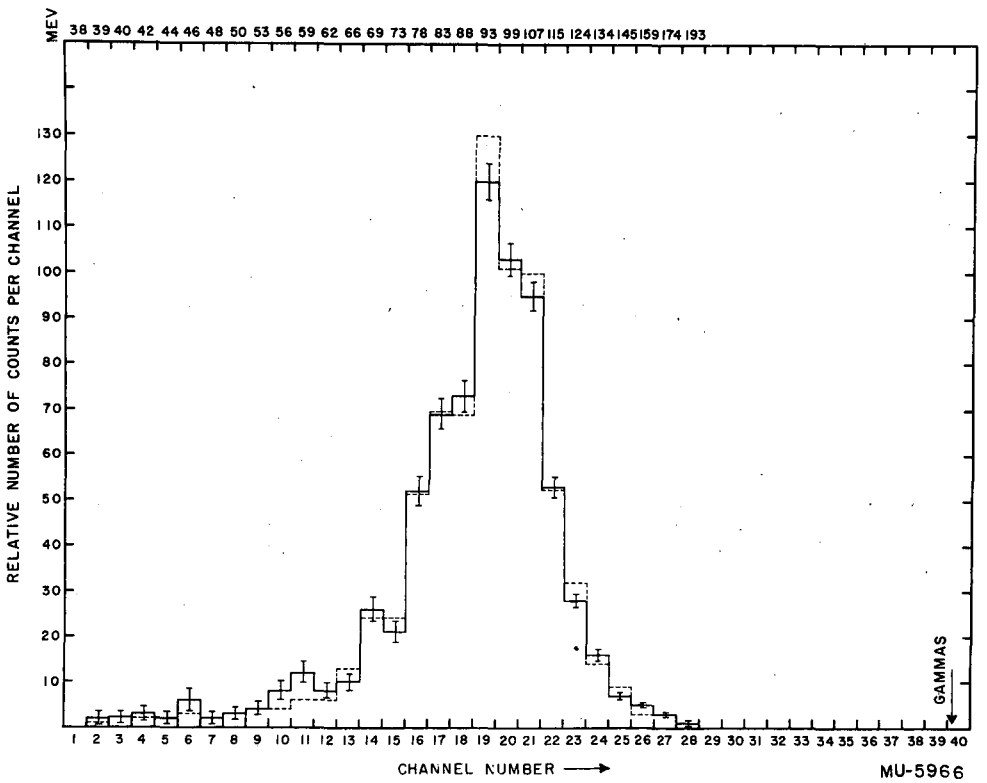

Fig. 11 Direct beam neutron spectrum (vs. time). 195 Mev deuterons are stripped on a copper probe 1 1/4 inches long. Ordinate is relative number of counts per channel one shake wide. Observed counts are corrected for "dead-time." (Correction is a few percent.) Calling this result N_a, the ordinate is $(N_a\, e^{\ell/\lambda})/\sigma_{np}$ where $e^{\ell/\lambda}$ is the scatterer attenuation and σ_{np} is the total n-p cross section. Abscissas are channel number (forty channels were "sensitive"), and neutron energy. Errors shown are standard deviations due to counting statistics only for carbon data. Solid curve refers to carbon, dotted curve refers to lead.

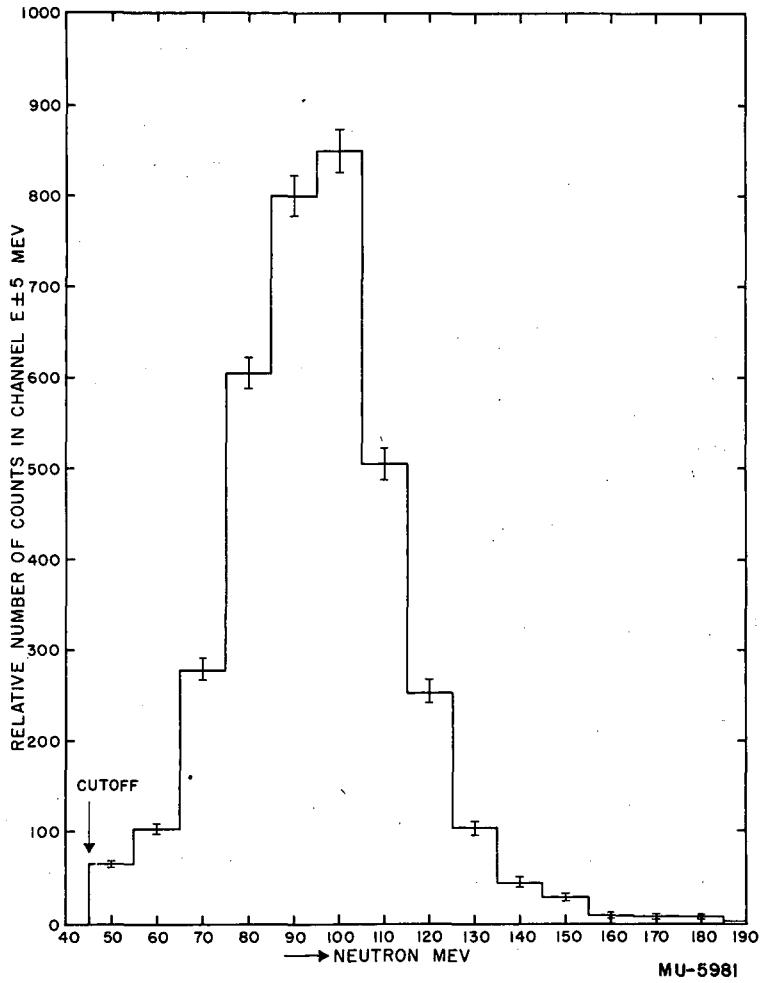

Fig. 12 Direct beam neutron spectrum (vs. energy). 195 Mev deuterons are stripped on a copper probe 1 1/4 inches long. Ordinate is relative number of counts per 10 Mev channel, obtained by graphical integration of Fig. 11. Errors shown are standard deviations, due to counting statistics only.

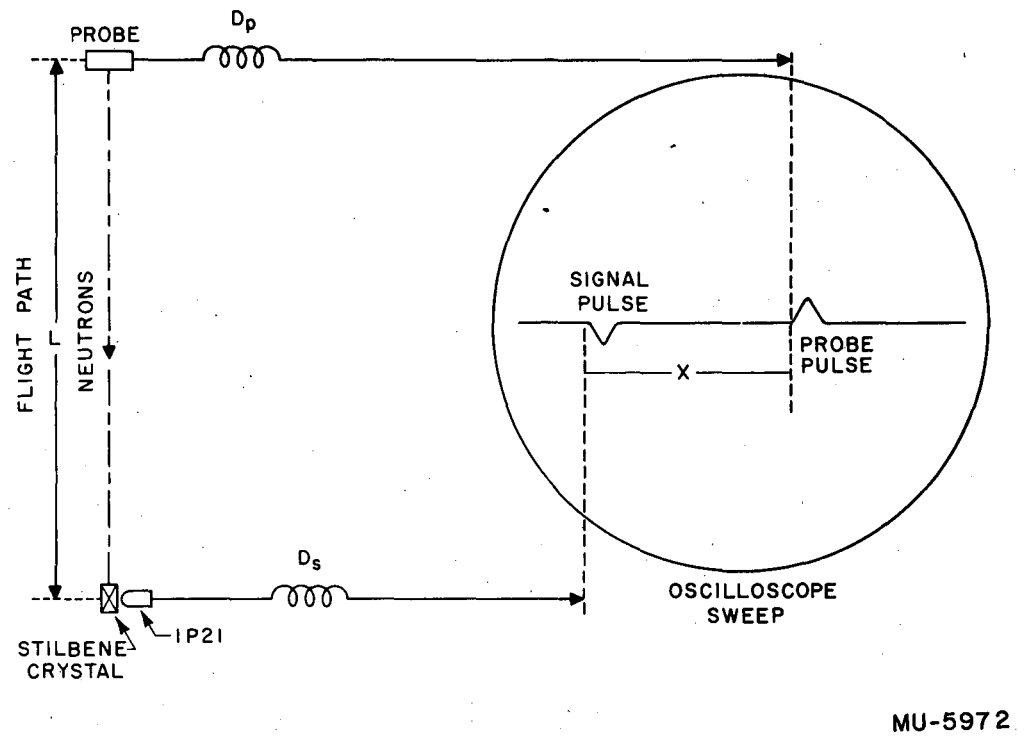

Fig. 13 Schematic diagram of circuit delays.

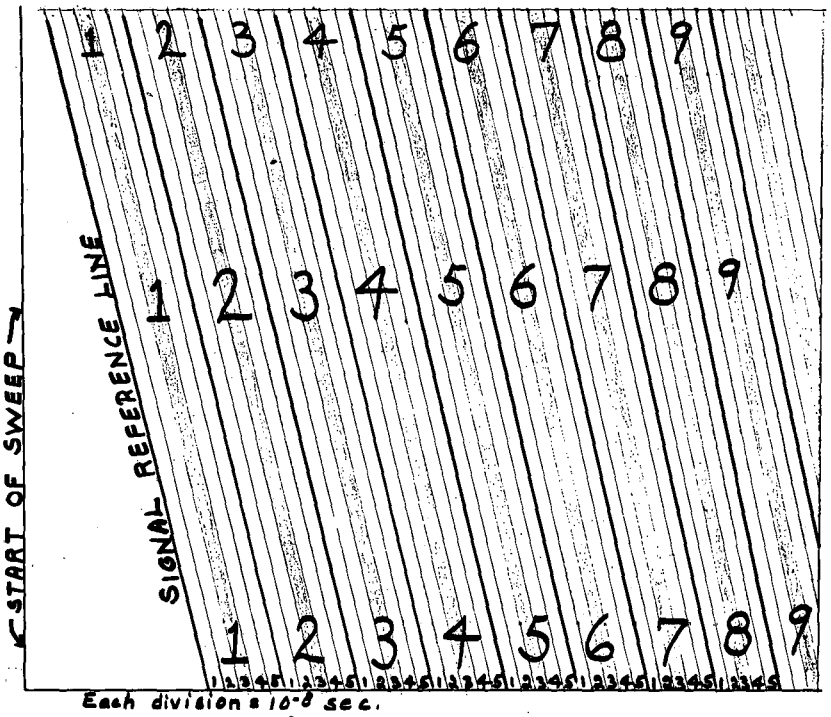

Fig. 14 Mat employed in film analysis. As used in viewer, mat was 48 cm. long, of which 35 cm. included the 40 one-shake channels.

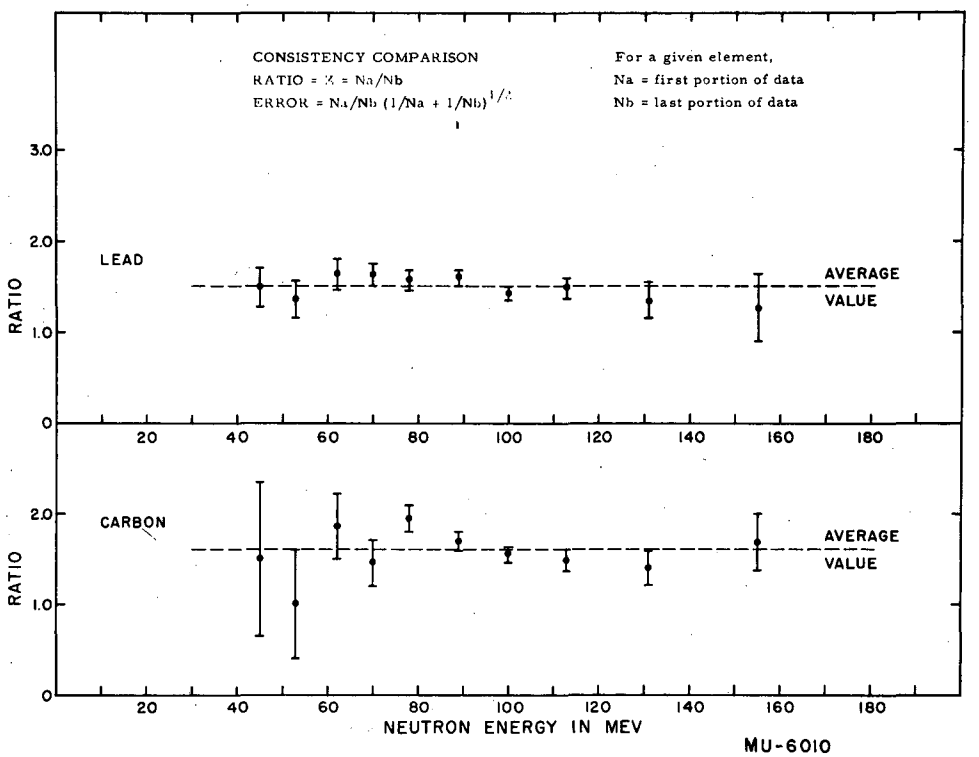

Fig. 15 Consistency comparison between reels for carbon and lead. Data for each element was divided into two portions. Ordinate gives ratio of the two portions, with error obtained from $(N_a/N_b)(N_a^{-1} + N_b^{-1})^{1/2}$. Abscissa refers to "energy"; i.e., same channel groupings as for regular data.

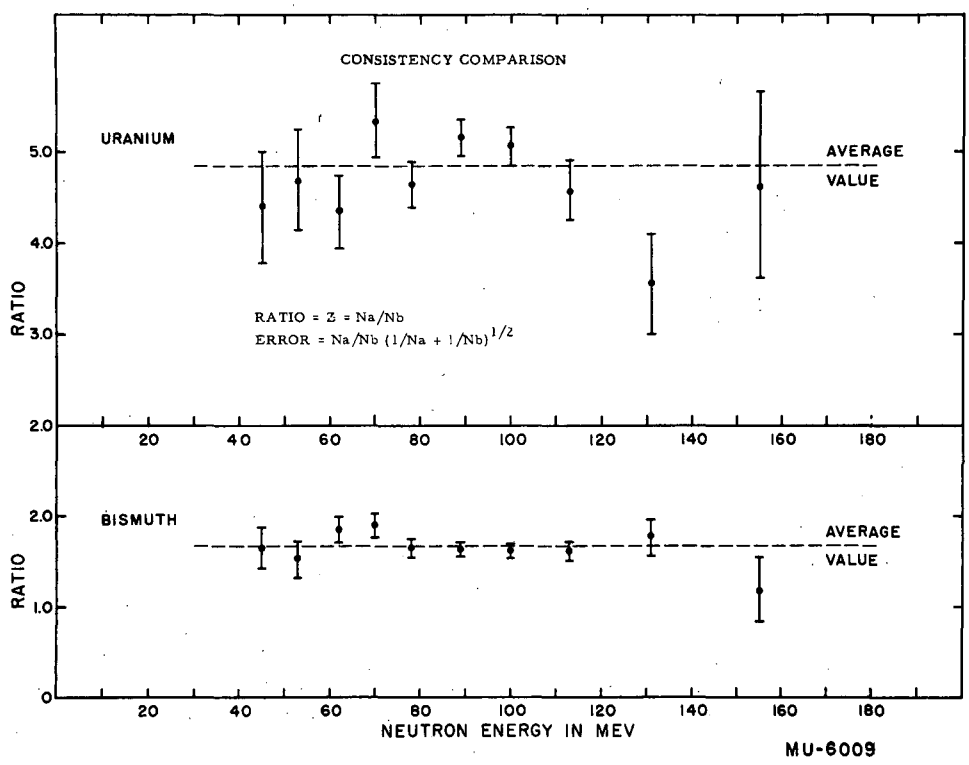

Fig. 16 Consistency comparison between reels for bismuth and uranium. Data for each element was divided into two portions. Ordinate gives ratio of the two portions, with error obtained from $(N_a/N_b)(N_a^{-1} + N_b^{-1})^{1/2}$. Abscissa refers to "energy"; i.e., same channel groupings as for regular data.

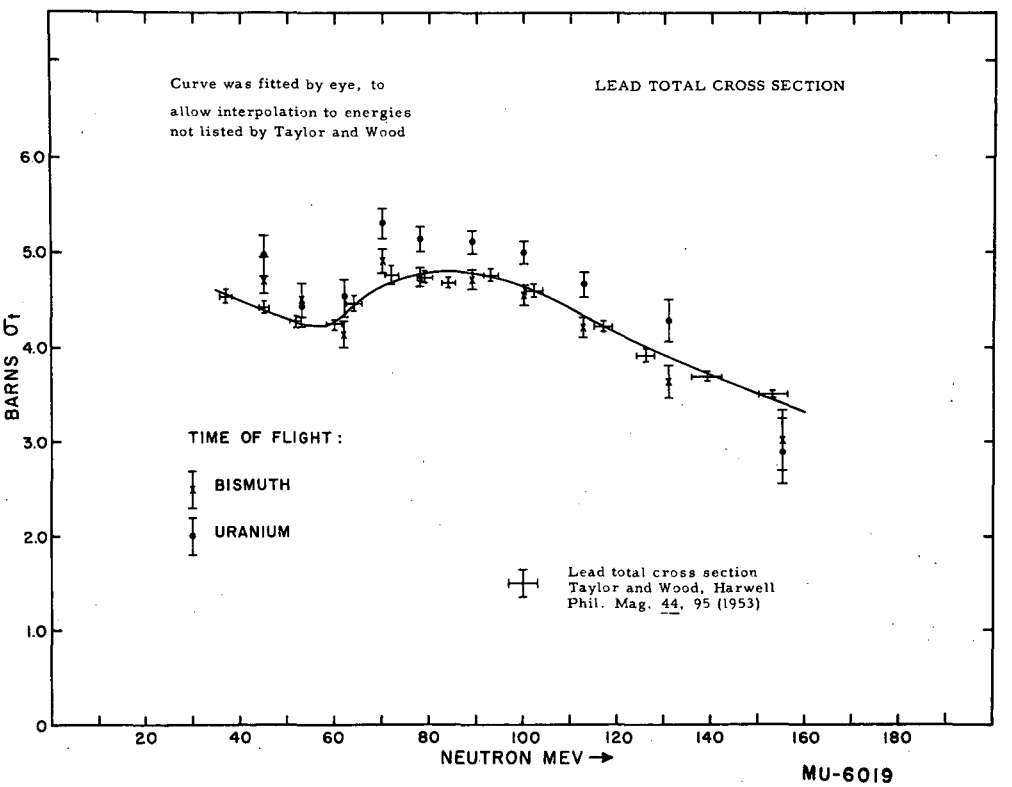

Fig. 17 Variation of total cross section of bismuth and uranium with energy. Curve shown was fitted by eye to data published by Taylor and Wood. Experimental points from this investigation have no adjustments in absolute value of cross section or energy. Error in energy is not shown; error in cross section is due to counting statistics only.

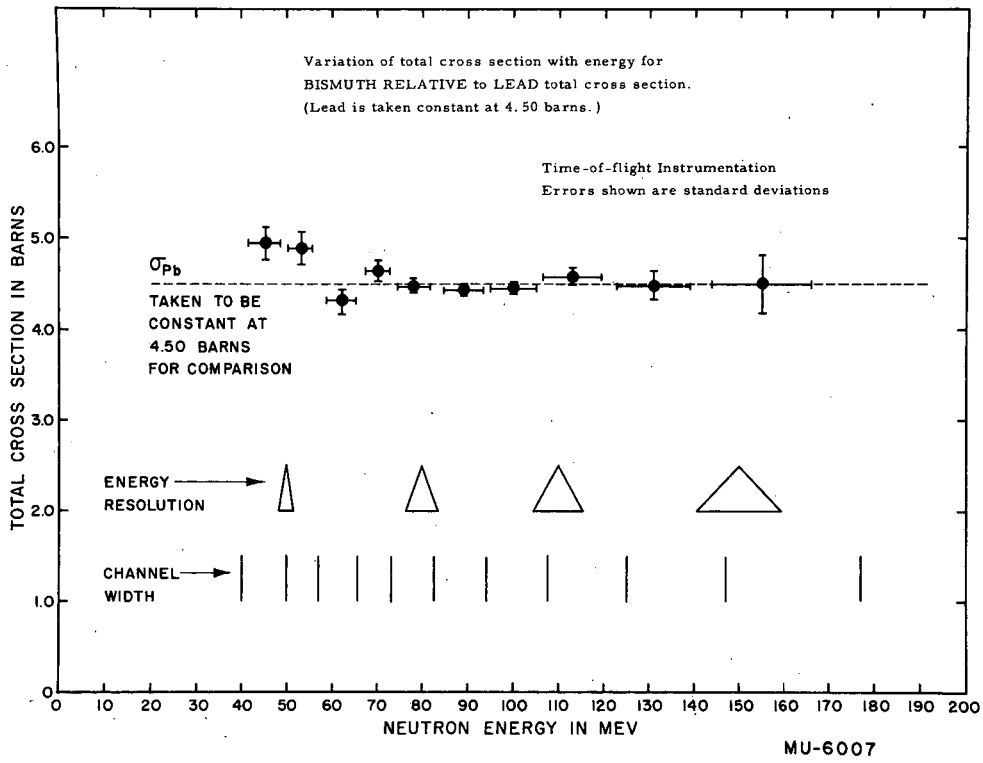

Fig. 18 Variation of total cross section with energy for bismuth relative to lead total cross section. Lead is taken constant at 4.50 barns for comparison. Errors shown are standard deviations.

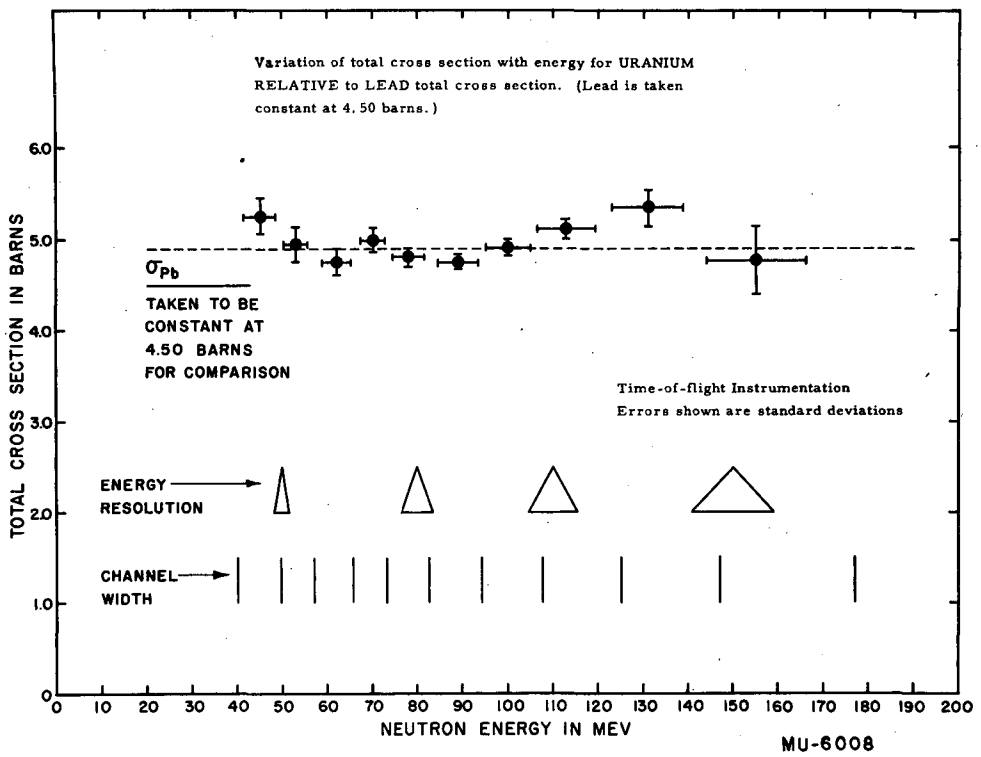

Fig. 19 Variation of total cross section with energy for uranium relative to lead total cross section. Lead is taken constant at 4.50 barns for comparison. Errors shown are standard deviations.

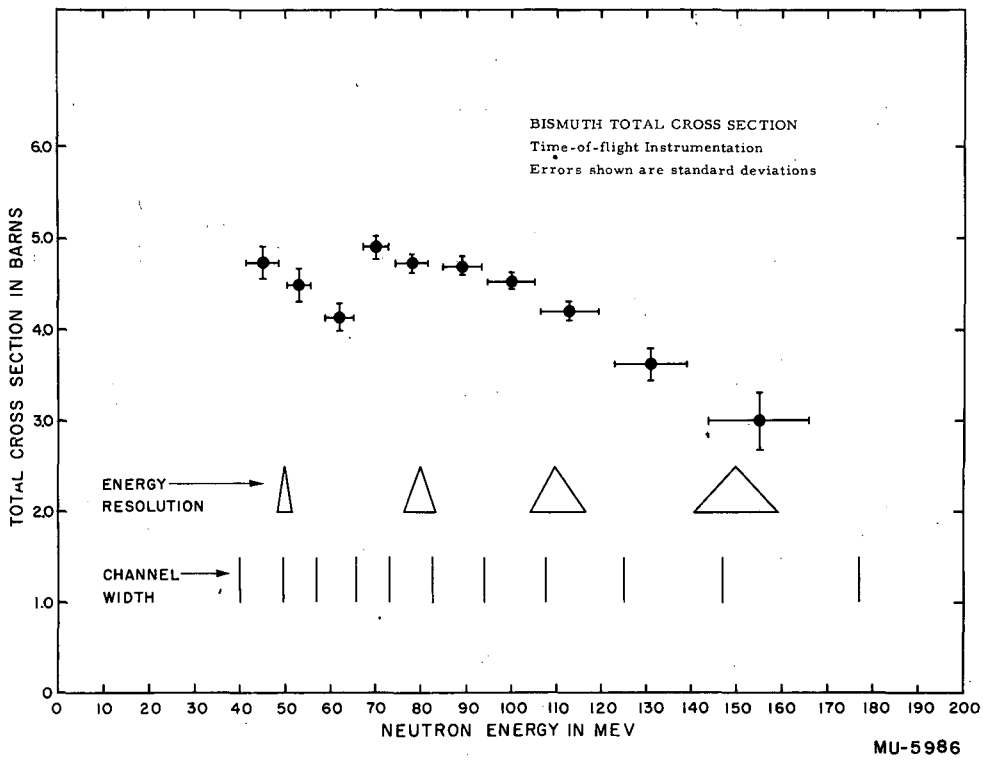

Fig. 20 Variation of total cross section of bismuth with energy. Errors shown are standard deviations.

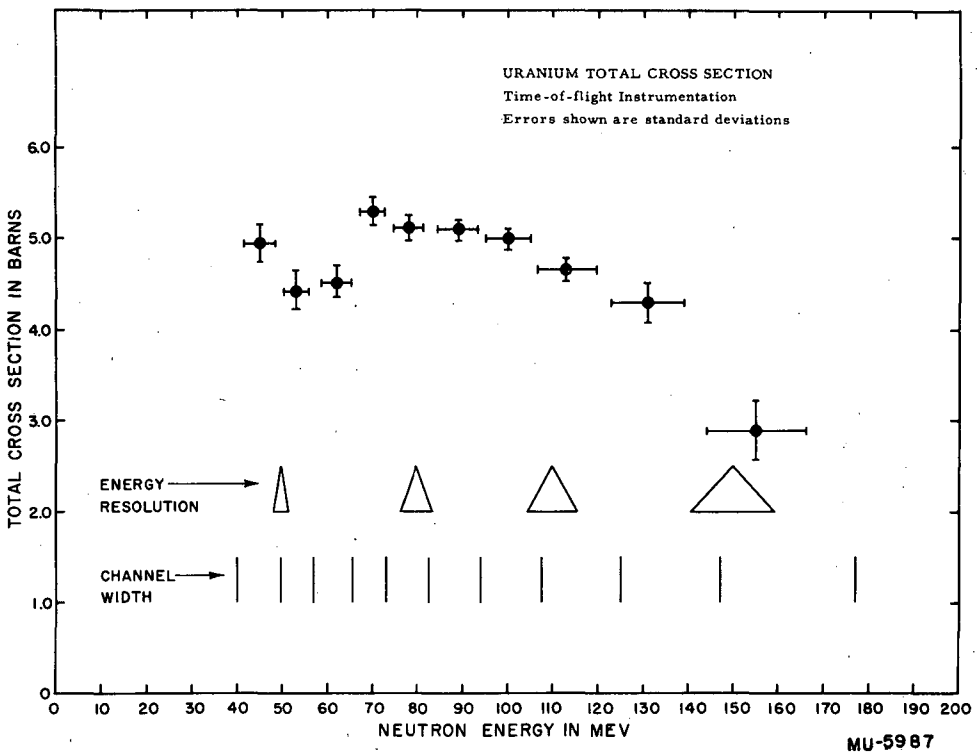

Fig. 21 Variation of total cross section of uranium with energy. Errors shown are standard deviations.

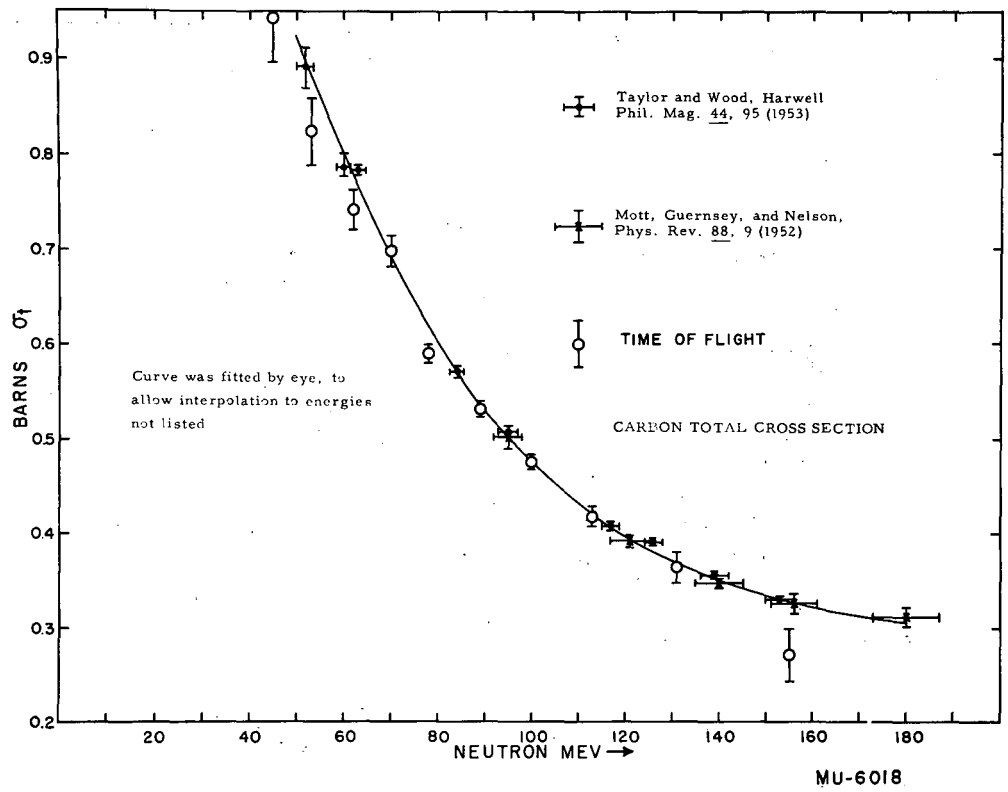

Fig. 22 Variation of total cross section of carbon with energy. Curve was fitted by eye to data published by Taylor and Wood, and by Mott, Guernsey, and Nelson. Experimental points from this investigation have no adjustments in absolute value of cross section or energy. Error in energy is not shown; error in cross section is due to counting statistics only.

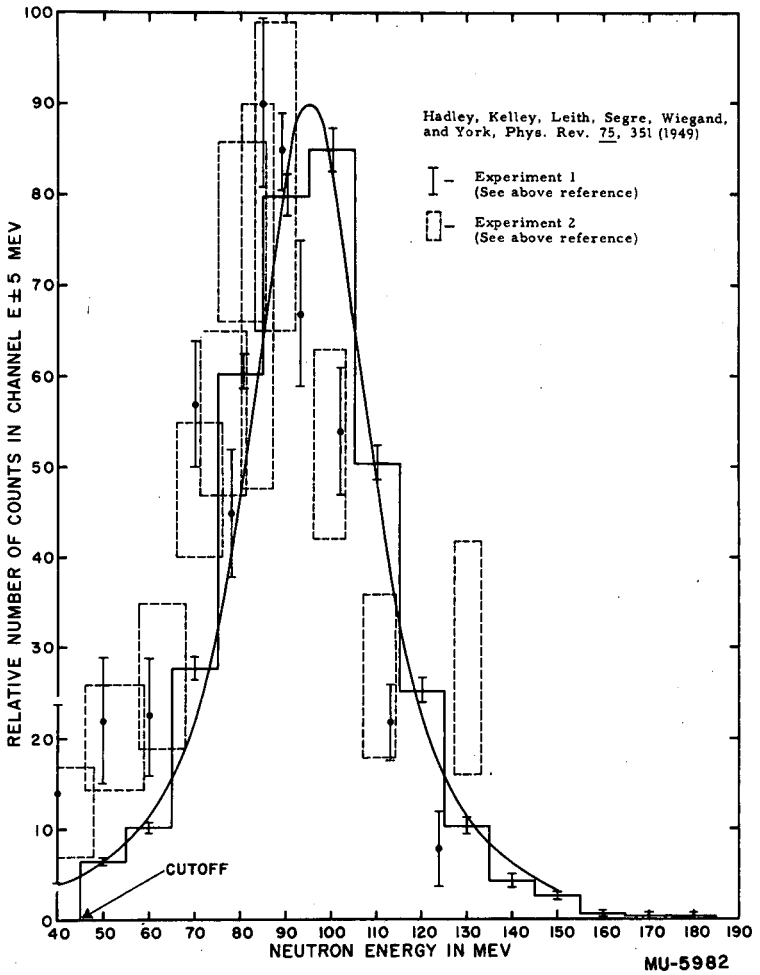

Fig. 23 Direct beam neutron spectrum compared to results published by others. Errors shown are standard deviations due to counting statistics. 195 Mev deuterons are stripped on copper probe 1 1/4 inches long.